Pendant Arm Functionalized Benzamidinate Titanium Imido Compounds: Experimental and Computational Studies of Their Reactions with CO_2

Catherine L. Boyd,[†] Eric Clot,*[,‡] Aldo E. Guiducci,[†] and Philip Mountford*[,†]

Chemistry Research Laboratory, University of Oxford, Mansfield Road, Oxford OX1 3TA, U.K., and LSDSMS (UMR 5636), cc 14, Université Montpellier 2, 34095 Montpellier Cedex 5, France

Received December 9, 2004

The syntheses of cyclopentadienyl titanium *tert*-butylimido complexes containing pendant arm functionalized amidinate ligands are reported, together with their reactions with CO_2. Mechanistic and DFT computational studies are also described. Reaction of [Ti(η-C_5R_4Me)(N^tBu)Cl(py)] (R = Me, H) with Li[$Me_3SiNC(Ph)N(CH_2)_nNMe_2$] ($n$ = 2, 3) afforded the corresponding (dimethylamino)ethylidene or -propylidene functionalized benzamidinate complexes [Ti(η-C_5R_4Me)(N^tBu){$Me_3SiNC(Ph)N(CH_2)_nNMe_2$}] (R = Me, n = 2 (**1**), 3 (**2**); R = H, n = 2 (**3**), 3 (**4**)). The n-propyl functionalized amidinate complex [Ti(η-C_5H_4Me)(N^tBu)-{$Me_3SiNC(Ph)NCH_2CH_2Me$}] (**5**) was also prepared for comparative purposes. The NMe_2 donors in **3** and **4** coordinate relatively weakly, and in solution the activation Gibbs free energy for NMe_2 dissociation for **3** is ca. 10 kJ mol^{-1} higher than that for **4**. All five compounds react with CO_2 to form the corresponding N,O-bound carbamate complexes [Ti(η-C_5R_4Me)-{$N^tBuC(O)O$}{$Me_3SiNC(Ph)NR'$}] (R = H, Me; R′ = $CH_2CH_2NMe_2$, $CH_2CH_2CH_2NMe_2$, CH_2CH_2Me), which, in turn, extrude ^{t}BuNCO (above −25 °C for R = H and at room temperature for R = Me) to form the μ-oxo-bridged dimeric complexes [Ti_2(η-C_5R_4Me)$_2$(μ-O)$_2${$Me_3SiNC(Ph)NR'$}$_2$], two of which have been structurally characterized. Only the C_5Me_5 carbamate complexes [Ti(η-C_5Me_5){$N^tBuC(O)O$}{$Me_3SiNC(Ph)N(CH_2)_nNMe_2$}] can be isolated and (for n = 3) structurally characterized. The reaction of **4** and **5** with CO_2 is spontaneous at −78 °C, whereas the corresponding reaction of **3** does not occur at significant rates below −35 °C. The rate of extrusion of ^{t}BuNCO from [Ti(η-C_5H_4Me){$N^tBuC(O)O$}{$Me_3SiNC(Ph)$-NR'] at −25 °C is twice as fast for R′ = $CH_2CH_2NMe_2$ as for $CH_2CH_2CH_2NMe_2$ and CH_2CH_2Me. DFT calculations have modeled the cycloaddition/extrusion reactions of **3**−**5** in conjunction with mechanistic and variable-temperature NMR experiments. The results show that the favored route is for the cycloaddition reaction to take place on 16-valence-electron, non pendant arm chelated isomers of **3** and **4** and that the relative ease of accessing these intermediates in fact controls the Ti=N^tBu/CO_2 coupling reaction.

Introduction

There continues to be much interest in the chemistry of terminal titanium imido compounds of the type $(L)_nTi{=}NR$, where $(L)_n$ represents a supporting ligand (set) and R is almost invariably an alkyl or aryl group.[1−12] An extensive reaction chemistry has now emerged from a large body of such derivatives supported by a range of supporting ligands. Although these compounds have proven potential in materials chemistry (as a source of TiN)[13−16] and olefin polymerization catalysis (Ti=NR acting as a "spectator ligand"),[17,18] it is the ability of the Ti=NR bond to act as a reactive site toward unsaturated substrates that has attracted the most attention. The list of potential substrates is now rather extensive and includes the follow-

* To whom correspondence should be addressed. E-mail: clot@univ-montp2.fr (E.C.); philip.mountford@chem.ox.ac.uk (P.M.).
† University of Oxford.
‡ Université Montpellier 2.

(1) Wigley, D. E. *Prog. Inorg. Chem.* **1994**, *42*, 239.
(2) Mountford, P. *Chem. Commun.* **1997**, 2127.
(3) Gade, L. H.; Mountford, P. *Coord. Chem. Rev.* **2001**, *216−217*, 65.
(4) Mountford, P. In *Perspectives in Organometallic Chemistry*; Royal Society of Chemistry: London, 2003.
(5) Pohlki, F.; Doye, S. *Chem. Soc. Rev.* **2003**, *32*, 104.
(6) Li, Y.; Shi, Y.; Odom, A. L. *J. Am. Chem. Soc.* **2004**, *126*, 1794.
(7) Basuli, F.; Bailey, B. C.; Huffman, J. C.; Mindiola, D. J. *Chem. Commun.* **2003**, 1554.
(8) Hanna, T. E.; Keresztes, I.; Lobkovsky, E.; Bernskoetter, W. H.; Chirik, P. J. *Organometallics* **2004**, *23*, 3448.
(9) Johnson, J. S.; Bergman, R. G. *J. Am. Chem. Soc.* **2001**, *123*, 2923.
(10) Bolton, P. D.; Mountford, P. *Adv. Synth. Catal.* **2005**, *347*, 355.
(11) Duncan, A. P.; Bergman, R. G. *Chem. Rec.* **2002**, *2*, 431.
(12) Straub, B. F.; Bergman, R. G. *Angew. Chem., Int. Ed.* **2001**, *40*, 4632.
(13) Winter, C. H.; Sheridan, P. H.; Lewkebandara, T. S.; Heeg, M. J.; Proscia, J. W. *J. Am. Chem. Soc.* **1992**, *114*, 1095.
(14) Lewkebandara, T. S.; Sheridan, P. H.; Heeg, M. J.; Rheingold, A. L.; Winter, C. H. *Inorg. Chem.* **1994**, *33*, 5879.
(15) McKarns, P. J.; Yap, G. P. A.; Rheingold, A. L.; Winter, C. H. *Inorg. Chem.* **1996**, *35*, 5968.
(16) Carmalt, C. J.; Newport, A.; Parkin, I. P.; Sealey, A. J.; Dubberley, S. R. *J. Mater. Chem.* **2003**, *13*, 84.
(17) Male, N. A. H.; Skinner, M. E. G.; Bylikin, S. Y.; Wilson, P. J.; Mountford, P.; Schröder, M. *Inorg. Chem.* **2000**, *39*, 5483.
(18) Adams, N.; Arts, H. J.; Bolton, P. D.; Cowell, D.; Dubberley, S. R.; Friedrichs, N.; Grant, C. M.; Kranenburg, M.; Sealey, A. J.; Wang, B.; Wilson, P. J.; Cowley, A. R.; Mountford, P.; Schröder, M. *Chem. Commun.* **2004**, 434.

10.1021/om049026f CCC: $30.25
Publication on Web 04/02/2005

Chart 1

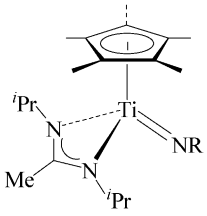

A

R = ^{t}Bu or 2,6-$C_6H_3Me_2$

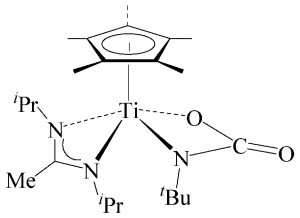

B

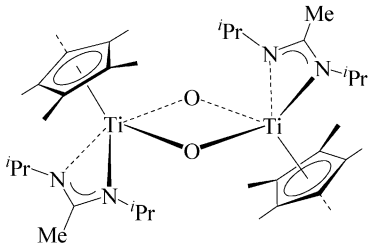

C

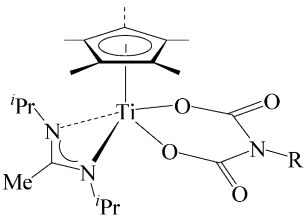

D

R = 2,6-$C_6H_3Me_2$

ing: alkenes,[19] alkynes,[6,20−22] allenes,[21] nitriles,[23] isonitriles,[24,25] and phosphaalkynes,[23,26−28] as well as isocyanates, CO_2, and other heterocumulenes.[29−33] The importance of titanium imido compounds as intermediates in hydroamination is also of note.[5,6,34−39] The reactions of Ti=NR groups with CO_2 are of the most relevance to our present contribution.

We have previously described the reactions of four types of titanium imido compounds (each featuring very different supporting ligand sets) with CO_2: [Ti(NR)(Me$_4$taa)] (Me$_4$taa = dianion of tetramethyldibenzotetraaza[14]annulene),[29] [Ti(NR)(Me$_2$calix)] (Me$_2$calix = the dianion of 1,3-dimethyl ether *p-tert*-butylcalix[4]arene),[30] [Ti(NR)(O_2NN′)] (H_2O_2NN′ = (2-C_5H_4N)CH_2N(2-HO-3,5-$C_6H_2{}^t$Bu$_2$)$_2$),[32] and [Ti(η-C_5Me$_5$)(NR){MeC(N^{i}Pr)$_2$}].[31] In all of these cases cycloaddition of CO_2 to the Ti=NR bond gives rise to a carbamate product of the type [(L)$_n$Ti{OC(O)N(R)}], although these are not always directly observed.[32] Depending on the identity of (L)$_n$ and R, the carbamates can in turn extrude the corresponding isocyanate RNCO via a cycloreversion process, forming either terminal (for (L)$_n$ = Me$_4$taa) or dimeric (for (L)$_n$ = Me$_2$calix, O_2NN′, (η-C_5Me$_5$){MeC(N^{i}Pr)$_2$}) titanium oxo side products. A detailed understanding of such bond-forming/bond-breaking reactions is important from the point of view of the controlled functionalization of CO_2 in particular[40−46] and for the design of useful group 4 imido complexes in general.

The reaction of the cyclopentadienyl−amidinate system [Ti(η-C_5Me$_5$)(NR){MeC(N^{i}Pr)$_2$}][31] (**A**; Chart 1) with CO_2 is particularly interesting, as it shows distinct selectivity as a function of the imido NR (R = ^{t}Bu, 2,6-$C_6H_3Me_2$) group. In the case when R = ^{t}Bu, CO_2 cycloaddition (to form the N,O-bound carbamate complex **B**) is followed by cycloreversion (extrusion of ^{t}BuNCO) to yield the dimeric oxo compound **C**, whereas the corresponding reaction for R = 2,6-$C_6H_3Me_2$ yields exclusively the double CO_2 activation product **D,** where a second CO_2 molecule inserts into the first-formed carbamate group Ti−N bond. Motivated by the potential of cyclopentadienyl−amidinate titanium imido complexes to offer further variation or control of CO_2 reactivity, we set out to develop pendant arm function-

(19) Bennett, J. L.; Wolczanski, P. T. *J. Am. Chem. Soc.* **1994**, *116*, 2179.
(20) Haak, E.; Bytsschkov, I.; Doye, S. *Angew. Chem., Int. Ed.* **1999**, *38*, 3389.
(21) Bashall, A.; Collier, P. E.; Gade, L. H.; McPartlin, M.; Mountford, P.; Trösch, D. J. M. *Chem. Commun.* **1998**, 2555.
(22) Ward, B. D.; Maisse-François, A.; Mountford, P.; Gade, L. H. *Chem. Commun.* **2004**, 704.
(23) Pugh, S. M.; Trösch, D. J. M.; Wilson, D. J.; Bashall, A.; Cloke, F. G. N.; Gade, L. H.; Hitchcock, P. B.; McPartlin, M.; Nixon, J. F.; Mountford, P. *Organometallics* **2000**, *19*, 3205.
(24) Blake, A. J.; Collier, P. E.; Gade, L. H.; McPartlin, M.; Mountford, P.; Schubart, M.; Scowen, I. J. *Chem. Commun.* **1997**, 1555.
(25) Bashall, A.; Collier, P. E.; Gade, L. H.; McPartlin, M.; Mountford, P.; Pugh, S. M.; Radojevic, S.; Schubart, M.; Scowen, I. J.; Trösch, D. J. M. *Organometallics* **2000**, *19*, 4784.
(26) Cloke, F. G. N.; Hitchcock, P. B.; Nixon, J. F.; Wilson, D. J.; Mountford, P. *Chem. Commun.* **1999**, 661.
(27) Cloke, F. G. N.; Hitchcock, P. B.; Nixon, J. F.; Wilson, D. J.; Tabellion, F.; Fischbeck, U.; Preuss, F.; Regitz, M.; Nyulaszi, L. *Chem. Commun.* **1999**, 2363.
(28) Asmus, S. M. F.; Regitz, M. *Tetrahedron Lett.* **2001**, *42*, 7543.
(29) Swallow, D.; McInnes, J. M.; Mountford, P. *J. Chem. Soc., Dalton Trans.* **1998**, 2253.
(30) Dubberley, S. R.; Friedrich, A.; Willman, D. A.; Mountford, P.; Radius, U. *Chem. Eur. J.* **2003**, *9*, 3634.
(31) Guiducci, A. E.; Cowley, A. R.; Skinner, M. E. G.; Mountford, P. *Dalton* **2001**, 1392.
(32) Boyd, C. L.; Toupance, T.; Tyrrell, B. R.; Ward, B. D.; Wilson, C. R.; Cowley, A. R.; Mountford, P. *Organometallics* **2005**, *24*, 309.
(33) Ong, T.-G.; Yap, G. P.; Richeson, D. S. *Chem. Commun.* **2003**, 2612.
(34) Nobis, M.; Drieβen-Hölscher, B. *Angew. Chem., Int. Ed.* **2001**, *40*, 3983.
(35) Tillack, A.; Jiao, H.; Castro, I. G.; Hartung, C. G.; Beller, M. *Chem. Eur. J.* **2004**, *10*, 2409.
(36) Ackermann, L.; Bergman, R. G.; Loy, R. N. *J. Am. Chem. Soc.* **2003**, *125*, 11956.
(37) Bytschkov, I.; Doye, S. *Eur. J. Org. Chem.* **2003**, 935.
(38) McGrane, P. L.; Jensen, M.; Livinghouse, T. *J. Am. Chem. Soc.* **1992**, *114*, 5459.
(39) McGrane, P. L.; Livinghouse, T. *J. Am. Chem. Soc.* **1993**, *115*, 11485.
(40) Darensbourg, D. J.; Kudaroski, R. A. *Adv. Inorg. Chem.* **1983**, *22*, 129.
(41) Palmer, D. A.; van Eldik, R. *Chem. Rev.* **1983**, *83*, 651.
(42) Arakawa, H. *Chem. Rev.* **2001**, *101*, 953.
(43) Torrent, M.; Sola, M.; Frenking, G. *Chem. Rev.* **2000**, *100*, 439.
(44) Leitner, W. *Coord. Chem. Rev.* **1996**, *153*, 257.
(45) Yin, X.; Moss, J. R. *Coord. Chem. Rev.* **1999**, *181*, 27.
(46) Gibson, D. *Chem. Rev.* **1996**, *96*, 2063.

Scheme 1. Synthesis of New Pendant Arm Cyclopentadienyl−Amidinate Titanium Imido Compounds

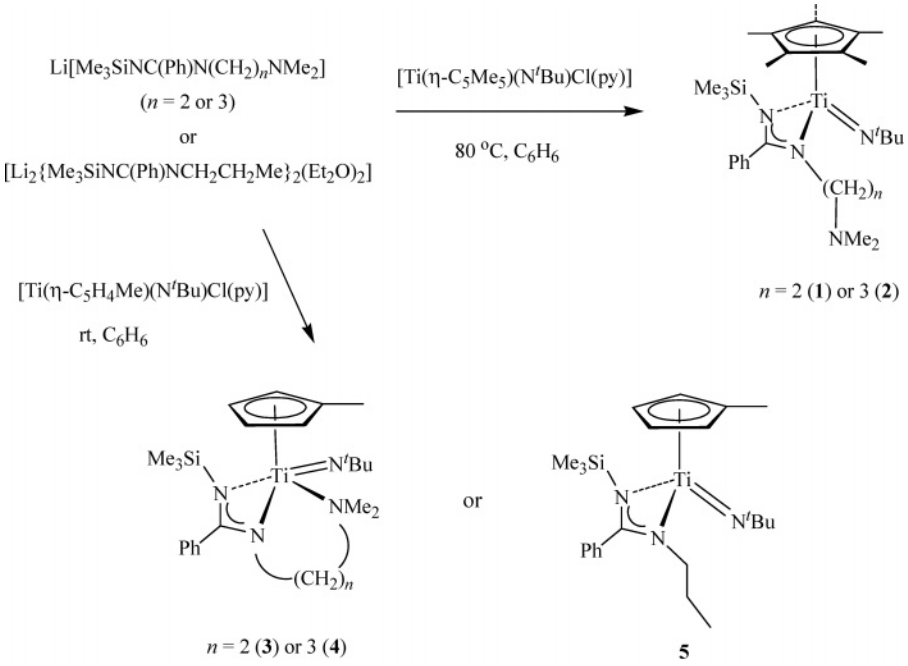

alized amidinate systems in order to probe the effect(s) of an additional hemilabile donor on the Ti=NR/CO_2 bond-making and bond-breaking reactions. In this contribution we employ two dimethylamino-functionalized benzamidinate ligands, namely $Me_3SiNC(Ph)NCH_2CH_2NMe_2$ (two methylene groups between the benzamidinate nitrogen and the NMe_2 group)[47] and $Me_3SiNC(Ph)NCH_2CH_2CH_2NMe_2$ (three carbon linker).[48] The two- and three-carbon linker systems allow us to establish the importance of the length of the pendant donor chain (and the size of the chelate ring that it might form). For comparison, we have also employed the approximately isosteric "dummy-arm" benzamidinate ligand[49,50] $Me_3SiNC(Ph)NCH_2CH_2Me$ (i.e., with no pendant donor group) in order to distinguish between steric and donor-group effects. We have reported recently on non-cyclopentadienyl titanium imido compounds containing these ligands.[49,51]

Results and Discussion

Synthesis of Cyclopentadienyl Pendant Arm Functionalized Amidinate *tert*-Butylimido Compounds. The starting compounds [Ti(η-C_5Me_5)(N^tBu)Cl(py)] and [Ti(η-C_5H_4Me)(N^tBu)Cl(py)] were prepared as previously described.[52] Reaction of [Ti(η-C_5Me_5)(N^tBu)Cl(py)] with Li[$Me_3SiNC(Ph)NCH_2CH_2NMe_2$] or Li[$Me_3SiNC(Ph)NCH_2CH_2CH_2NMe_2$] in C_6H_6 at 80 °C yielded the new compounds [Ti(η-C_5Me_5)(N^tBu){$Me_3SiNC(Ph)NCH_2CH_2NMe_2$}] (**1**) and [Ti($\eta$-$C_5Me_5$)($N^tBu$){$Me_3SiNC(Ph)NCH_2CH_2CH_2NMe_2$}] (**2**) in 83% and 89% yields, respectively (Scheme 1). The ^1H and $^{13}C\{^1H\}$ NMR spectra for **1** and **2** support the proposed structures. Without coordination of the pendant NMe_2 group, **1** and **2** are formally 16-valence-electron complexes. Coordination of NMe_2 would form an 18-valence-electron compound and also render the methyl groups of the NMe_2 moiety chemically inequivalent. ^1H NMR spectra for both compounds at room temperature feature a singlet (6 H) for the NMe_2 protons, indicating that either the pendant arm is not coordinated to the metal center or that methyl group exchange is fast on the NMR time scale at this temperature. Cooling NMR samples of **1** and **2** to −90 °C in CD_2Cl_2 (500.1 MHz ^1H resonance frequency) revealed some broadening of the NMe_2 resonance but did not result in splitting into two separate resonances. Therefore, the pendant NMe_2 groups in **1** and **2** probably coordinate very weakly to the metal but even at low temperatures easily dissociate. This was confirmed by the observation of only one resonance for the NMe_2 methyls in the $^{13}C\{^1H\}$ NMR spectra at −95 °C.

Corresponding reactions of [Ti(η-C_5H_4Me)(N^tBu)Cl(py)] with the lithiated pendant amine functionalized amidinates or with the "dummy arm" amidinate [Li_2\{$Me_3SiNC(Ph)NCH_2CH_2Me$\}$_2$(Et_2O)$_2$] in C_6H_6 afforded the compounds [Ti(η-C_5H_4Me)(N^tBu){$Me_3SiNC(Ph)NCH_2CH_2NMe_2$}] (**3**), [Ti($\eta$-$C_5H_4Me$)($N^tBu$){$Me_3SiNC(Ph)NCH_2CH_2CH_2NMe_2$}] (**4**), and [Ti($\eta$-$C_5H_4Me$)($N^tBu$){$Me_3SiNC(Ph)NCH_2CH_2Me$}] (**5**) in good crude yields (Scheme 1). These three compounds are oils at room temperature and could only be purified by high-vacuum distillation (1×10^{-5} mbar, 120−130 °C). The room-temperature ^1H NMR spectra of compounds **3**−**5** are analogous to those of **1** and **2**. However, cooling samples of **3** and **4** in CD_2Cl_2 revealed decoalescence points for the NMe_2 singlets at 237 ± 2 and 208 ± 2 K, respectively, below which two distinct NMe resonances were observed. This indicates that the NMe_2 groups in **3** and

(47) Brandsma, M. J. R.; Brussee, E. A. C.; Meetsma, A.; Hessen, B.; Teuben, J. H. *Eur. J. Inorg. Chem.* **1998**, 1867.
(48) Doyle, D.; Gun'ko, Y. K.; Hitchcock, P. B.; Lappert, M. F. *Dalton* **2000**, 4093.
(49) Boyd, C. L.; Guiducci, A. E.; Dubberley, S. R.; Tyrrell, B. R.; Mountford, P. *Dalton* **2002**, 4175.
(50) Boyd, C. L.; Tyrrell, B. R.; Mountford, P. *Acta Crystallogr.* **2002**, *E58*, m597.
(51) Croft, A. C. R.; Boyd, C. L.; Cowley, A. R.; Mountford, P. *J. Organomet. Chem.* **2003**, *683*, 120.
(52) Dunn, S. C.; Mountford, P.; Robson, D. A. *J. Chem. Soc., Dalton Trans.* **1997**, 293.

4 coordinate to titanium in the ground state, giving two chemically distinct Me group environments (eq 1), and

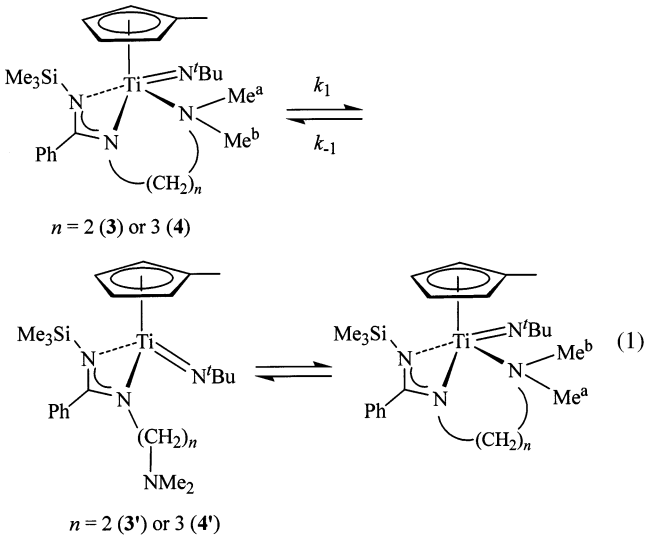

(1)

is confirmed by the presence of two NMe resonances in the low-temperature $^{13}C\{^1H\}$ NMR spectra of these compounds. For **4** an NOE was observed at −90 °C between the NMe resonances and the ^{t}Bu group of the imido ligand, confirming coordination of the NMe_2 group. Coordination of the pendant arm to titanium may be more favorable for the C_5H_4Me systems than for the C_5Me_5 systems **1** and **2**, since C_5Me_5 is both more sterically demanding and electron releasing.

Although it is likely that the NMe_2 methyls (arbitrarily labeled "Me^a" and "Me^b") of **3** and **4** undergo mutual chemical exchange via the 16-valence-electron isomers **3′** and **4′**, no evidence for significant equilibrium amounts of either of these compounds was indicated by any of the low-temperature spectra. Therefore, assuming that ^1H NMR could detect a minimum of ca. 1% of **3′** (or **4′**) in the presence of a 99% relative amount of **3** (or **4**) (i.e. $K_{eq} = [\mathbf{3'}]/[\mathbf{3}]$ or $[\mathbf{4'}]/[\mathbf{4}] \leq 0.01$), then k_{-1} (eq 1) must be at least 2 orders of magnitude greater than k_1 for both the **3/3′**and **4/4′** dynamic equilibria (since $K_{eq} = k_1/k_{-1}$). Furthermore, a K_{eq} value of ≤0.01 would imply that ΔG_{rxn} for the process **3** → **3′** and **4** → **4′** must be ca. ≥10 kJ mol^{-1} at temperatures below −40 °C.

Activation Parameters for NMe_2 Methyl Group Exchange in 3 and 4. The values of $\Delta G^{\ddagger}_{T_c}$ (Gibbs free energy of activation at the coalescence temperature T_c) from coalescence measurements of the NMe_2 resonances of **3** and **4** in the ^1H NMR spectra (at 237 ± 2 and 208 ± 2 K, respectively) were extracted using standard procedures[53] and are listed in Table 1. Strictly speaking, the $\Delta G^{\ddagger}_{T_c}$ values refer to the highest barrier to overcome on the Gibbs free energy surface to effectively exchange Me^a and Me^b. This process could be described as three consecutive steps: NMe_2 dissociation, inversion at NMe_2, and rotation about the CH_2-NMe_2 σ bond. However, it is very likely that all processes are coupled and the actual TS for exchange would be best described as a concomitant dissociation of NMe_2 and reorganization of the pendant arm to achieve Me exchange. However, the NMe_2 group must dissociate sufficiently

Table 1. Values of $\Delta G^{\ddagger}_{T_c}$ (from ^1H Coalescence Measurements) and Activation Parameters $\Delta H^{\ddagger}$ and $\Delta S^{\ddagger}$ (from Variable-Temperature ^1H Linewidth Analysis) for NMe_2 Methyl Group Exchange for [Ti(η-C_5H_4Me)(N^tBu){$Me_3SiNC(Ph)NCH_2CH_2NMe_2$}] (3) and [Ti($\eta$-$C_5H_4Me$)($N^tBu$)-{$Me_3SiNC(Ph)NCH_2CH_2CH_2NMe_2$}] (4)

compd	T_c (K)	$\Delta G^{\ddagger}_{T_c}$ (kJ mol^{-1})	$\Delta H^{\ddagger}$ (kJ mol^{-1})	$\Delta S^{\ddagger}$ (J mol^{-1} K^{-1})
3	237 ± 2	46.4 ± 0.4	81.2 ± 7.1	150 ± 30
4	208 ± 2	41.6 ± 0.4	95 ± 27	267 ± 133

enough to permit inversion at the nitrogen, and so it is reasonable to assume that the Me exchange involves the 16-electron isomers **3′** and **4′**. Such process are expected to have positive $\Delta S^{\ddagger}$ values.[54] $\Delta G^{\ddagger}_{T_c}$ values obtained at different T_c's cannot be directly compared because of the different $T_c\Delta S^{\ddagger}$ contributions, but since T_c (208 ± 2 K) for the three-carbon linker compound **4** ($\Delta G^{\ddagger}_{208} = 41.6 \pm 0.4$ kJ mol^{-1}) is ca. 30 K lower than that for the two-carbon linker compound **3** ($\Delta G^{\ddagger}_{237} = 46.4 \pm 0.4$ kJ mol^{-1}), the $\Delta G^{\ddagger}_{T_c}$ value for **4** would be even lower than the value given in Table 1 at the T_c for **3**. Overall, it seems very likely that $\Delta G^{\ddagger}$ for NMe_2 dissociation will be significantly lower at any particular temperature for **4** than for **3**.

To gain an additional insight into the activation parameters, we attempted to obtain $\Delta H^{\ddagger}$ and $\Delta S^{\ddagger}$ (and hence $\Delta G^{\ddagger}$) values from ^1H NMR (500.1 MHz) NMe_2 line width measurements at temperatures below the coalescence temperature for both compounds. Activation parameters for NMe group exchange in **3** and **4** were obtained by ^1H NMR (500.1 MHz) line width analysis at 3 K intervals at temperatures between 215 and 233 K (for **3**) and between 186 and 201 K (for **4**) in CD_2Cl_2. In each case, the line widths at half-height ($\nu_{1/2}$(obs)) were corrected by subtracting the natural line widths obtained from the low-temperature-limit ^1H NMR spectrum at 183 K. These corrected values ($\nu_{1/2}$(corr)) were used to calculate the observed rate constants for the processes Me^a → Me^b {k_{obs}(a→b)} and Me^b → Me^a {k_{obs}(b→a)} according to $k_{obs} = \pi\nu_{1/2}$(corr).[53,55] The rate constants were used to construct Eyring plots (see the Supporting Information), assuming that the rate constant k_1 (eq 1) is equal to $2k_{obs}$, since the conversion of the methyl group environment "a" to "b" occurs at the same rate as the conversion from environment "b" to "a". Values for $\Delta H^{\ddagger}$ and $\Delta S^{\ddagger}$ were extracted and are listed in Table 1.

It is clear from Table 1 that there are rather large errors on the enthalpic and entropic activation data for both systems. This arises unavoidably from the difficulty in obtaining good-quality spectra at the very low temperatures required. The errors are particularly large for the three-carbon linker system **4**. Although one therefore cannot make detailed comparisons of the $\Delta H^{\ddagger}$ and $\Delta S^{\ddagger}$ values between the two compounds **3** and **4**, it is indisputable that the NMe_2 methyl group exchange processes are associated with significantly positive $\Delta S^{\ddagger}$ values. Likewise, the $\Delta H^{\ddagger}$ data are favorably comparable

(53) Sandström, J. *Dynamic NMR Spectroscopy*; Academic Press: London, 1982.

(54) For a general account of thermodynamic aspects of chelate ring opening processes, see: Hancock, R. D.; Martell, A. E. *Chem. Rev.* **1989**, *89*, 1875.

(55) Green, M. L. H.; Wong, L.-L.; Sella, A. *Organometallics* **1992**, *11*, 2660.

Scheme 2. Reactions of [Ti(η-C_5Me_5)(N^{t}Bu){$Me_3SiNC(Ph)N(CH_2)_nNMe_2$}] ($n$ = 2 (1), 3 (2)) with CO_2

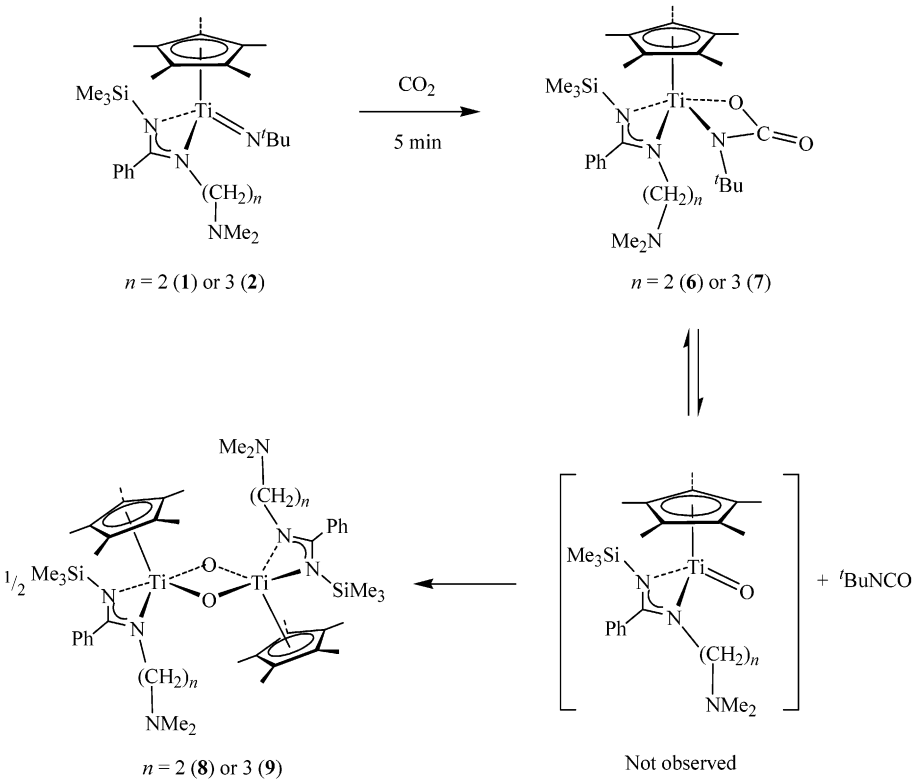

to those for related dissociative equilibria of amidinate-supported titanium imido complexes.[56]

As a check on the internal consistency between the $\Delta G^{\ddagger}$ values for **4** obtained from coalescence and line width analyses, it is reassuring that the $\Delta G^{\ddagger}$ values for **4** at 237 K (T_c) extracted from coalescence (46.4 ± 0.4 kJ mol^{-1}) and the Eyring plots (45.6 ± 14.1 kJ mol^{-1}) are in good agreement, despite the large errors on the activation parameters extracted from the line width data.

To make a comparison between $\Delta G^{\ddagger}$ for both systems at the same temperature, the more precise activation parameters extracted for the two-carbon linker system **3** have been used to calculate $\Delta G^{\ddagger}_{208}$ (208 K being T_c for the three-carbon linker system **4**), which can then be compared to $\Delta G^{\ddagger}_{208}$ for **4** calculated directly from the coalescence measurement. The values thus obtained are $\Delta G^{\ddagger}_{208}$ = 50.0 ± 13.2 kJ mol^{-1} for **3** and 41.6 ± 0.4 kJ mol^{-1} for **4**. These data are consistent with there being a smaller $\Delta G^{\ddagger}_{208}$ value for dissociation of the three-carbon linker arm in **4** than for the two-carbon linker arm in **3**. While the data in Table 1 do not permit us to determine the origin of this effect with any certainty, it seems likely that it might be the result of a greater gain in entropy upon dissociation of a three-carbon arm from the metal.[54]

Reactions of C_5Me_5 Compounds 1 and 2 with CO_2. Reaction of the compounds [Ti(η-C_5Me_5)(N^{t}Bu){$Me_3SiNC(Ph)NCH_2CH_2NMe_2$}] (**1**) and [Ti($\eta$-$C_5Me_5$)(N^{t}Bu){$Me_3SiNC(Ph)NCH_2CH_2CH_2NMe_2$}] (**2**) with CO_2 (1 atm) at room temperature for 5 min, followed by immediate isolation, yielded the cherry red N,O-bound carbamates [Ti(η-C_5Me_5){N^{t}BuC(O)O}{$Me_3SiNC(Ph)NCH_2CH_2NMe_2$}] (**6**) and [Ti($\eta$-$C_5Me_5$){N^{t}BuC(O)O}{$Me_3SiNC(Ph)NCH_2CH_2CH_2NMe_2$}] (**7**) in 76% and 82% isolated yields, respectively (Scheme 2). The carbamate complexes **6** and **7** give rise to the expected ^{1}H and ^{13}C spectra, and their IR spectra contain bands at 1686 and 1666 cm^{-1}, respectively, which are attributed to ν(C=O) of the carbamate ligand.[31,57] The single-crystal X-ray structure of **7** is discussed below.

The cycloaddition products **6** and **7** are unstable in solution and decompose over ca. 1 h with elimination of ^{t}BuNCO, as identified by ^{1}H NMR spectroscopy, to form the oxo compounds **8** and **9**. The absence of terminal Ti=O stretches in the range 850−930 cm^{-1} in the IR spectra of these products suggests that they are dimeric μ-oxo species, namely [Ti_2(η-C_5Me_5)$_2$(μ-O)$_2${$Me_3SiNC(Ph)NCH_2CH_2NMe_2$}$_2$] (**8**) and [$Ti_2$($\eta$-$C_5Me_5$)$_2$($\mu$-O)$_2${$Me_3SiNC(Ph)NCH_2CH_2CH_2NMe_2$}$_2$] (**9**). This is supported by the dimeric structures found by X-ray crystallography for the methylcyclopentadienyl μ-oxo complexes **10a** and **11a** (vide infra). The dimeric non pendant arm acetamidinate analogue [Ti_2(η-C_5Me_5)$_2$(μ-O)$_2${$MeC(N^iPr)_2$}$_2$] (**C**; Chart 1) has also been crystallographically characterized.[31] The oxo compounds **8** and **9** are highly insoluble, and neither NMR data nor mass spectral data could be obtained.

The proposed mechanism for this process involves a retrocyclization (Scheme 2) to form initially a terminal oxo complex (possibly with NMe_2 coordination). No evidence was observed for this species in the NMR-scale reactions, suggesting that it immediately undergoes back-reaction with ^{t}BuNCO (re-forming **6** or **7**) or eventually self-traps irreversibly by dimerization to give **8** or **9**. This is in contrast to the reactions of CO_2 with

(56) Stewart, P. J.; Blake, A. J.; Mountford, P. *Inorg. Chem.* **1997**, *36*, 3616.

(57) Blake, A. J.; McInnes, J. M.; Mountford, P.; Nikonov, G. I.; Swallow, D.; Watkin, D. J. *J. Chem. Soc., Dalton Trans.* **1998**, 379.

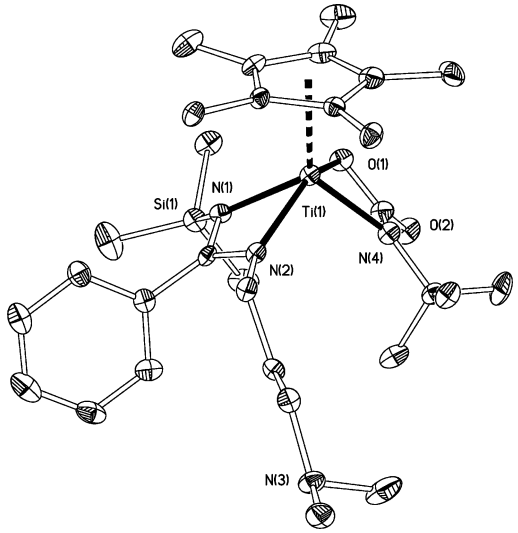

Figure 1. Displacement ellipsoid plot of [Ti(η-C_5Me_5)-{N^{t}BuC(O)O}{Me_3SiNC(Ph)N$CH_2CH_2CH_2NMe_2$}] (**7**) (25% probability). H atoms are omitted for clarity.

Table 2. Selected Bond Lengths (Å) and Angles (deg) for [Ti(η-C_5Me_5){N^{t}BuC(O)O}-{Me_3SiNC(Ph)N$CH_2CH_2CH_2NMe_2$}] (7)[a]

Ti(1)−Cp_{cent}	2.058	Ti(1)−N(4)	1.991(5)
Ti(1)−N(1)	2.087(5)	Ti(1)−O(1)	1.971(4)
Ti(1)−N(2)	2.131(4)		
Cp_{cent}−Ti(1)−N(1)	119.3	Cp_{cent}−Ti(1)−N(4)	129.3
Cp_{cent}−Ti(1)−N(2)	108.7	Cp_{cent}−Ti(1)−O(1)	109.0

[a] Cp_{cent} refers to the computed C_5Me_5 ring centroid.

the dibenzotetraaza[14]annulene-supported titanium imides [Ti(NR)(Me_4taa)].[29] In these systems, extrusion of RNCO (R = ^{t}Bu, aryl) from the intermediate carbamates yields stable terminal titanium oxo compounds. Decomposition of **6** and **7** via ^{t}BuNCO extrusion to form oxo products **8** and **9** is much faster for these pendant arm functionalized systems (ca. 1 h) than for the previously reported non pendant arm acetamidinate system [Ti(η-C_5Me_5){N^{t}BuC(O)O}{MeCN(^{i}Pr)$_2$}], which takes ca. 12 h to completely decompose to the corresponding dimeric oxo product. This possibly suggests that the pendant donor group may play a role in the extrusion step (an anchimeric effect[58]). Alternatively, the difference in steric demands of the N substituents of the two different amidinate ligands may be responsible.

The molecular structure of compound **7** is shown in Figure 1, and selected bond distances and angles are presented in Table 2. The pendant arm is clearly not coordinated, and the compound has a pseudo four-legged piano-stool structure that is slightly distorted, as revealed by the Cp_{cent}−Ti−N and −O angles (Table 2). The Cp_{cent}−Ti(1)−N(1) angle is 119.3°, as compared to a Cp_{cent}−Ti(1)−N(2) angle of 108.7°. Similarly, the Cp_{cent}−Ti(1)−N(4) angle is 129.3°, while the Cp_{cent}−Ti(1)−O(1) angle is 109.0°. This is probably due to unfavorable steric interactions between the C_5Me_5 ring and the bulky ^{t}Bu and $SiMe_3$ groups. Unfavorable steric interactions between these groups also explain the formation of the observed isomer, in which the ^{t}Bu and $SiMe_3$ groups are trans to each other, as confirmed by the observation of only one isomer in the ^{1}H NMR spectrum. The distances and angles associated with the Ti{OC(O)N} moiety are comparable to those in the dibenzotetraaza[14]annulene-supported carbamate [Ti{N(4-C_6H_4Me)C(O)O}(Me_4taa)].[29]

Reactions of C_5H_4Me Compounds 3−5 with CO_2 at Room Temperature. The behavior of the methylcyclopentadienyl systems **3**−**5** was found to differ significantly from that of the C_5Me_5 systems **1** and **2**. Upon exposure to CO_2 at room temperature a color change to cherry red was observed straight away but the color darkened to brown almost immediately, indicating decomposition to the corresponding oxo compound. When the reaction was followed at room temperature by ^{1}H NMR spectroscopy, spectra after 5 min contained resonances attributable to both the imido starting materials and the dimeric oxo products [Ti_2(η-C_5H_4Me)$_2$(μ-O)$_2${Me_3SiNC(Ph)NR}$_2$] (R = $CH_2CH_2NMe_2$ (**10**), $CH_2CH_2CH_2NMe_2$ (**11**), CH_2CH_2Me (**12**)), together with ^{t}BuNCO, but not the expected carbamate intermediates **13**−**15**. This is in contrast to the reactions (Scheme 2) of the C_5Me_5 systems **1** and **2**; these display only resonances due to the intermediate carbamate under the same reaction time and conditions. The immediate decomposition of the proposed carbamate intermediates **13**−**15** means that characterization is not possible at room temperature. The faster rate of their decomposition in comparison to that of the C_5Me_5 compounds **1** and **2** is attributed to the decreased steric stabilization toward dimerization of a transient monomeric oxo intermediate provided by C_5H_4Me compared to C_5Me_5. Scheme 3 summarizes the overall sequence for the reaction of **3**−**5** with CO_2.

The dimeric oxo products **10**−**12** have been isolated and characterized by NMR and IR spectroscopy and mass spectrometry. The NMR spectra were found to contain twice as many resonances as expected for single products and probably imply the formation of both trans and cis isomers (**10a**−**12a** and **10b**−**12b**; Scheme 3). It was found that heating samples to 80 °C in C_6D_6 for several hours led to a shift in the relative ratios of the two products in favor of the trans isomer. Single crystals of the trans isomers **10a** and **11a** were grown from solutions in pentane at room temperature. The molecular structures are shown in Figure 2, and selected bond lengths and angles are listed in Tables 3 and 4.

The structures of **10a** and **11a** confirm that they are μ-oxo dimers and that the NMe_2 groups do not coordinate to the metal. Both compounds have a pseudo four-legged piano-stool geometry about the titanium atoms. Compounds with $Ti_2(\mu\text{-O})_2$ cores are well established, and several have been crystallographically characterized.[59,60] The bond lengths and angles are of comparable magnitudes for the two compounds. Both compounds have slightly asymmetric $Ti_2(\mu\text{-O})_2$ cores in which the Ti−O bond trans to the $SiMe_3$-bearing nitrogen is slightly longer than the Ti−O bond trans to the pendant arm bearing nitrogen. This may be attributed to the asymmetric amidinate ligand substitution, as the symmetric oxo dimer [Ti_2(η-C_5H_4Me)$_2$(μ-O)$_2${PhC($NSiMe_3$)$_2$}$_2$]

(58) Braunstein, P.; Naud, F. *Angew. Chem., Int. Ed.* **2001**, *40*, 680.

(59) Allen, F. H.; Kennard, O. *Chem. Des. Automation News* **1993**, *8*, 1&31.

(60) Fletcher, D. A.; McMeeking, R. F.; Parkin, D. J. *J. Chem. Inf. Comput. Sci.* **1996**, *36*, 746.

Scheme 3. Reactions of [Ti(η-C_5H_4Me)(N^tBu){$Me_3SiNC(Ph)N(CH_2)_nNMe_2$}] ($n$ = 2 (3), 3 (4)) and [Ti(η-C_5H_4Me)(N^tBu){$Me_3SiNC(Ph)NCH_2CH_2Me$}] (5) with CO_2

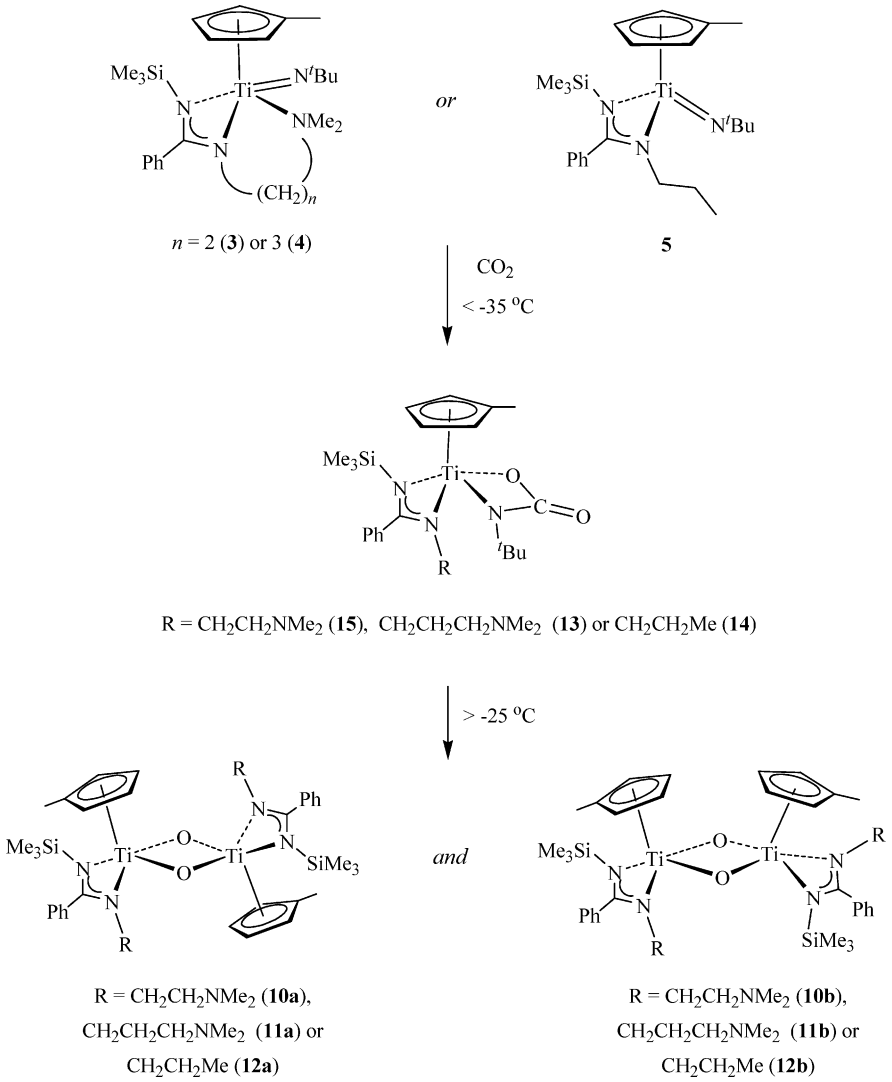

(**C**; Chart 1) has equal bond lengths for both Ti−O and Ti−$N_{amidinate}$ bonds.[31]

Reactions of C_5H_4Me Compounds 3−5 with CO_2: Low-Temperature Studies. Reactions of **3**−**5** with CO_2 at −78 °C revealed a difference in behavior between the two-carbon and the three-carbon pendant arm systems **3** and **4**. When an NMR tube sample of **4** in CD_2Cl_2 at −78 °C was exposed to CO_2 (ca. 1 atm), the ^1H NMR spectrum (−78 °C) recorded immediately afterward contained only resonances attributable to the carbamate [Ti(η-C_5H_4Me){$N^tBuC(O)O$}{$Me_3SiNC(Ph)$-$NCH_2CH_2CH_2NMe_2$}] (**13**; Scheme 3). Subsequent warming of this solution to −25 °C led to extrusion of ^{t}BuNCO and the trans and cis dimeric oxo compounds **11**. This behavior was mirrored by the "dummy-arm" compound **5**, which gave carbamate **14** immediately at −78 °C and then extrusion of isocyanate at −25 °C to form the oxo compounds **12**. However, when the two-carbon pendant arm compound **3** was exposed to CO_2 at −78 °C, the ^1H NMR spectrum showed only resonances for **3**. Cycloaddition to form the carbamate [Ti(η-C_5H_4Me){N^tBuC-$(O)O$}{$Me_3SiNC(Ph)NCH_2CH_2NMe_2$}] (**15**) did not occur at a significant rate until the solution was warmed to −35 °C. Further warming to −25 °C resulted in isocyanate extrusion to yield the dimeric oxo compounds **10**. This extrusion occurred at a rate which appeared to be qualitatively about twice as fast as for **13** and **14** at the same temperature. Note that the −78 °C NMR spectra of **13** and **15** showed no evidence of NMe_2 group coordination and in this regard these compounds are analogous to the C_5Me_5 homologues **6** and **7**.

These observations suggested that the NMe_2 donor in the pendant arm systems could influence both the rate of cycloaddition of CO_2 to the Ti=N^tBu bond of **3** and the extrusion of ^{t}BuNCO from the carbamate intermediates. Low-temperature kinetic studies were therefore carried out to probe the role of the pendant donor group during the various stages of the reactions of **3**−**5** with CO_2.

Cycloaddition Reaction of 3 with CO_2: Kinetic and Mechanistic Studies. Low-temperature control of the cycloaddition of CO_2 to the Ti=N^tBu bond of **3** makes this reaction convenient for determining the rate law dependence of CO_2 in the reaction to form the carbamate **15**. These studies were carried out under pseudo-first-order conditions, whereby at least a 10-fold excess of CO_2 was present at the lowest pressure studied (linear $\ln(I/I_0)$ plots (e.g. Figure 3b and the Supporting Information) showed no evidence for significant diffusion control limitations in these experiments). NMR

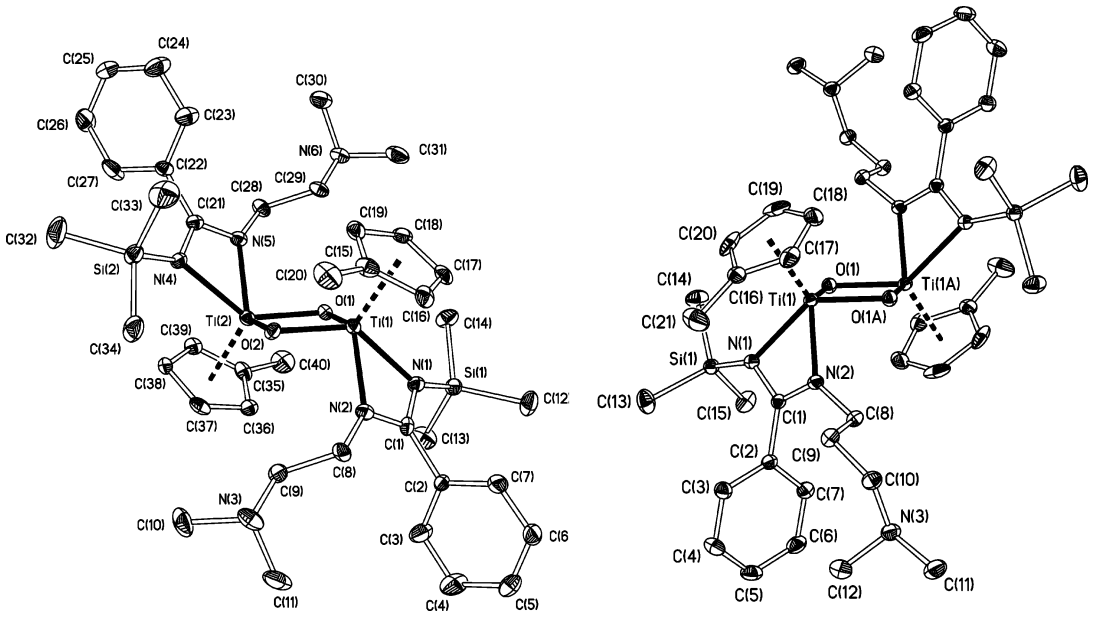

Figure 2. Displacement ellipsoid plots of (a, left) one of the crystallographically independent molecules of *trans*-[$Ti_2(\eta$-$C_5H_4Me)_2(\mu$-$O)_2${$Me_3SiNC(Ph)NCH_2CH_2NMe_2$}$_2$] (**10a**) (20% probability) and (b, right) *trans*-[$Ti_2(\eta$-$C_5H_4Me)_2(\mu$-$O)_2${$Me_3SiNC(Ph)NCH_2CH_2CH_2NMe_2$}$_2$] (**11a**) (25% probability). H atoms are omitted for clarity. For **11a**, atoms carrying the suffix "A" are related to their counterparts by the symmetry operator $-x, -y + 1, -z + 1$.

Table 3. Selected Bond Lengths (Å) and Angles (deg) for *trans*-[$Ti_2(\eta$-$C_5H_4Me)_2(\mu$-$O)_2$-{$Me_3SiNC(Ph)NCH_2CH_2NMe_2$}$_2$] (10a)[a]

Ti(1)−N(1)	2.180(6)	Ti(2)−N(4)	2.202(6)
Ti(1)−N(2)	2.123(6)	Ti(2)−N(5)	2.116(7)
Ti(1)−$Cp_{cent(1)}$	2.081	Ti(2)−$Cp_{cent(2)}$	2.08
Ti(1)−O(1)	1.813(5)	Ti(2)−O(1)	1.897(5)
Ti(1)−O(2)	1.892(5)	Ti(2)−O(2)	1.813(5)
$Cp_{cent(1)}$−Ti(1)−N(1)	108.5	$Cp_{cent(2)}$−Ti(1)−N(4)	107.9
$Cp_{cent(1)}$−Ti(1)−N(2)	110.9	$Cp_{cent(2)}$−Ti(1)−N(5)	111.9
$Cp_{cent(1)}$−Ti(1)−O(1)	121.6	$Cp_{cent(2)}$−Ti(1)−O(1)	111.7
$Cp_{cent(1)}$−Ti(1)−O(2)	112.2	$Cp_{cent(2)}$−Ti(1)−O(2)	122.2

[a] $Cp_{cent(1)}$ and $Cp_{cent(2)}$ refer to the computed C_5H_4Me ring centroids for Ti(1) and Ti(2), respectively.

Table 4. Selected Bond Lengths (Å) and Angles (deg) for *trans*-[$Ti_2(\eta$-$C_5H_4Me)_2(\mu$-$O)_2$-{$Me_3SiNC(Ph)NCH_2CH_2NMe_2$}$_2$] (11a)[a]

Ti(1)−N(1)	2.203(1)	Ti(1)−O(1)	1.802(1)
Ti(1)−N(2)	2.096(1)	Ti(1)−O(1A)	1.907(1)
Ti(1)−Cp_{cent}	2.086		
Cp_{cent}−Ti(1)−N(1)	109.6	Cp_{cent}−Ti(1)−O(1)	121.7
Cp_{cent}−Ti(1)−N(2)	115.6	Cp_{cent}−Ti(1)−O(1A)	111.3

[a] Cp_{cent} refers to the computed C_5H_4Me ring centroid. Atoms carrying the suffix "A" are related to their counterparts by the symmetry operator $-x, -y + 1, -z + 1$.

samples of **3** in CD_2Cl_2 were exposed to known pressures of CO_2 at −78 °C. Samples were transferred to a spectrometer with a probe maintained at the same temperature. The sample was warmed to −35 °C, at which temperature cycloaddition occurred at a significant rate and NMR spectra were recorded over at least 3 half-lives. The reaction was carried out at four CO_2 pressures in the range 0.25−1.0 atm. The relative concentrations of the imido starting material **3** and the carbamate **15** were measured from each spectrum, and the results were fitted to a first-order exponential relationship. The observed rate constant k_{obs} was extracted from a plot of $\ln(I/I_0)$ vs time for **3** (parts a and b of Figure 3) The k_{obs} data are summarized in Table 5,

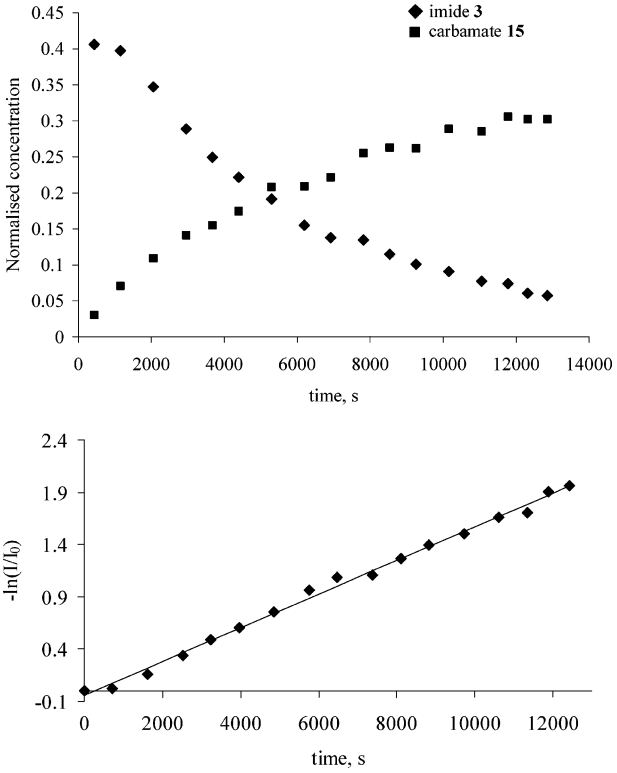

Figure 3. (a, top) Plot of normalized concentrations vs time for the cycloaddition reaction of **3** with CO_2 (0.5 atm) Values given are for the starting imide [Ti(η-C_5H_4Me)-(N^tBu){$Me_3SiNC(Ph)NCH_2CH_2NMe_2$}] (**3**) and product carbamate [Ti(η-C_5H_4Me){$OC(O)N^tBu$}{$Me_3SiNC(Ph)NCH_2$-CH_2NMe_2}] (**15**). (b, bottom) Plot of $\ln(I/I_0)$ vs time for the reaction of [Ti(η-C_5H_4Me)(N^tBu){$Me_3SiNC(Ph)NCH_2CH_2$-NMe_2}] (**3**) with CO_2 (0.5 atm).

and further details are given in the Supporting Information. The exponential decay of the starting material and evolution of carbamate indicate that the rate-determining step is a bimolecular reaction which is first

Table 5. Observed Rate Constants k_{obs} for Cycloaddition of CO_2 to [Ti(η-C_5H_4Me)(N^{t}Bu){$Me_3SiNC(Ph)NCH_2CH_2NMe_2$}] (3) at Different CO_2 Pressures

$p(CO_2)$ (atm)	$k_{obs} \times 10^4$ (s^{-1})	$p(CO_2)$ (atm)	$k_{obs} \times 10^4$ (s^{-1})
0.25	0.74 ± 0.02	0.75	2.7 ± 0.03
0.50	1.6 ± 0.03	1.0	3.7 ± 0.04

order in CO_2. This is confirmed by the linear dependence of k_{obs} on CO_2 pressure (Figure 4, Table 5).

Scheme 4 summarizes the two likely mechanisms for addition of CO_2 to the pendant arm compounds **3** and **4**. In mechanism 1, cycloaddition of CO_2 to the imide takes place without decoordination of the pendant arm from the metal. Mechanism 2 involves a preequilibrium in which the pendant arm dissociates from the metal to generate an intermediate species (**3′** or **4′**), which then undergoes cycloaddition of CO_2. Note that for the "dummy arm" imide **5** a simple bimolecular process analogous to the second step of mechanism 2 is the only possibility.

For mechanism 1, the rate law is given by eq 2 (where "imide" = **3** or **4**).

$$\text{rate} = k[\text{imide}][CO_2] \quad (2)$$

Under pseudo-first-order conditions (large and effectively constant $[CO_2]$ as in the experiments described above), this expression approximates to eq 3, where $k_{obs} = k[CO_2]$ and is linearly dependent upon $[CO_2]$.

$$\text{rate} = k_{obs}[\text{imide}] \quad (3)$$

The rate law for mechanism 2 may be derived by applying the steady-state approximation to the intermediates **3′** and **4′** such that the rate law in eq 4 applies (k_1, k_{-1}, and k_2 as defined in eq 1 and Scheme 4).

$$\text{rate} = \frac{k_1 k_2[\text{imide}][CO_2]}{k_{-1} + k_2[CO_2]} \quad (4)$$

However, in the case where $k_{-1} \gg k_2[CO_2]$, eq 4 approximates to eq 5, where $k'_{obs} = (k_1k_2/k_{-1})[CO_2]$ and again has a linear dependence on $[CO_2]$.

$$\text{rate} = k'_{obs}[\text{imide}] \quad (5)$$

Therefore, the experimental data for the reaction of **3** with CO_2 fit either mechanism 1 (eq 3) or mechanism 2 (eq 5), provided that k_{-1} is larger than $k_2[CO_2]$. This issue is further addressed using DFT calculations later in this paper.

Extrusion of ^{t}BuNCO: Mechanistic and Kinetic Studies. Given the very different rates of cycloaddition of CO_2 to Ti=N^{t}Bu for the two-carbon and three-carbon arm NMe_2 donor systems **3** and **4**, it was of interest to quantify any anchimeric effect of the different arms on the rate of ^{t}BuNCO extrusion.

Extrusion of ^{t}BuNCO from all three carbamates **13**−**15** to form the bridging oxo products (Scheme 3) was monitored by low-temperature NMR at the same concentrations. The isosteric "dummy arm" system **14** was used as a control to benchmark any effect of the pendant $(CH_2)_nNMe_2$ donors upon the rate of extrusion. All of the NMR studies were carried out on in situ generated

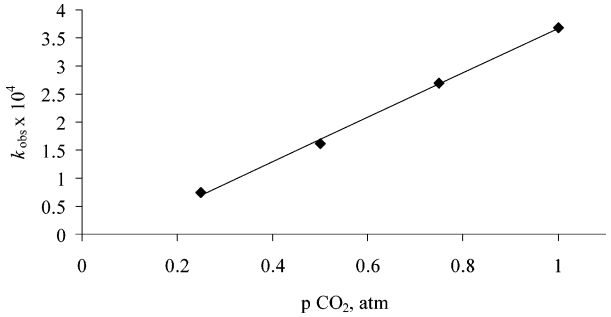

Figure 4. Plot of k_{obs} vs CO_2 pressure for the reaction of [Ti(η-C_5H_4Me)(N^{t}Bu){$Me_3SiNC(Ph)NCH_2CH_2NMe_2$}] (**3**) with CO_2 at −35 °C.

carbamates (vide supra). Additional studies were made on the "dummy-arm" system (**14** → **12**) at three different concentrations, to probe the dependence of the rate of decomposition upon carbamate concentration (since compounds **13**−**15** are monomeric and the ultimate products **10**−**12** are dimeric, it is possible that the rate-determining step could be bimolecular with respect to titanium). The experiments for **13** and **15** were carried out in duplicate and were highly reproducible. NMR samples of in situ generated **13**−**15** were warmed to −30 °C, at which point all of the imido starting materials had been consumed by reaction with CO_2 and only carbamate was present.[61] Extrusion of ^{t}BuNCO from the carbamates **13**−**15** to yield **10**−**12** was followed over 3 half-lives of carbamate. The data were fitted to a first-order exponential relationship. The rate constants k extracted from plots of $\ln(I/I_0)$ vs. time (Figure 5 shows data for **13** by way of example) are listed in Table 6.

The data (Table 6) for extrusion from **14** show that the reaction is independent of [**14**] in the range studied; therefore, a bimolecular rate-limiting step is unlikely.[62] Examination of the rate constants for **13**−**15** reveals a small but persistent increase in the rate constant for extrusion with the two-carbon arm system **15** compared with **13** and **14**. Energetically the effect is small (2−3 kJ mol^{-1} difference in $\Delta G^{\ddagger}$ for extrusion), but nonetheless it amounts to a quantitatively established halving of the half-life ($t_{1/2}$, Table 6) for extrusion on going from the three-carbon arm system **13** to the two-carbon arm system **15**. This effect might arise from slight differences in steric effects between the two ligands or from a small anchimeric effect of the ligand arm. The compounds **13** (three-carbon arm) and **14** ("dummy" arm) have experimentally indistinguishable values for k, suggesting that the three-carbon arm NMe_2 does not accelerate measurably the rate of ^{t}BuNCO extrusion from the carbamate. Attempts to address this issue via DFT studies are described in the following section.

Density Functional Theory Computational Studies. Transition-metal imido compounds have been the subject of several computational studies, as this ligand is involved in various catalytic transformations.[63] They

(61) In the case of the two-carbon linker carbamate **15**, a small amount of imido starting material **3** was still present at −25 °C and data obtained until all of this had been consumed were discarded.

(62) It has recently been shown that the transient terminal titanium oxo compound [Ti(η-C_5Me_5)(O){$MeC(N^iPr)_2$}] generated by ^{t}BuNCO extrusion from the unstable carbamate B (Chart 1) can be trapped using *p*-tolyl isocyanate, forming a double-substrate activation product somewhat analogous to that in: Boyd, C. L. D. Phil. Thesis, University of Oxford, 2004.

(63) Cundari, T. R., *Chem. Rev.*, **2000**, 100, 807.

Scheme 4. Two Alternative Mechanisms for the Formation of Carbamates 15 and 13 from the Starting Imido Complexes 3 or 4 on Reaction with CO_2: (Mechanism 1) Cycloaddition at the Complex with the NMe_2 Group Coordinated; (Mechanism 2): Dissociation of NMe_2 Precedes Cycloaddition

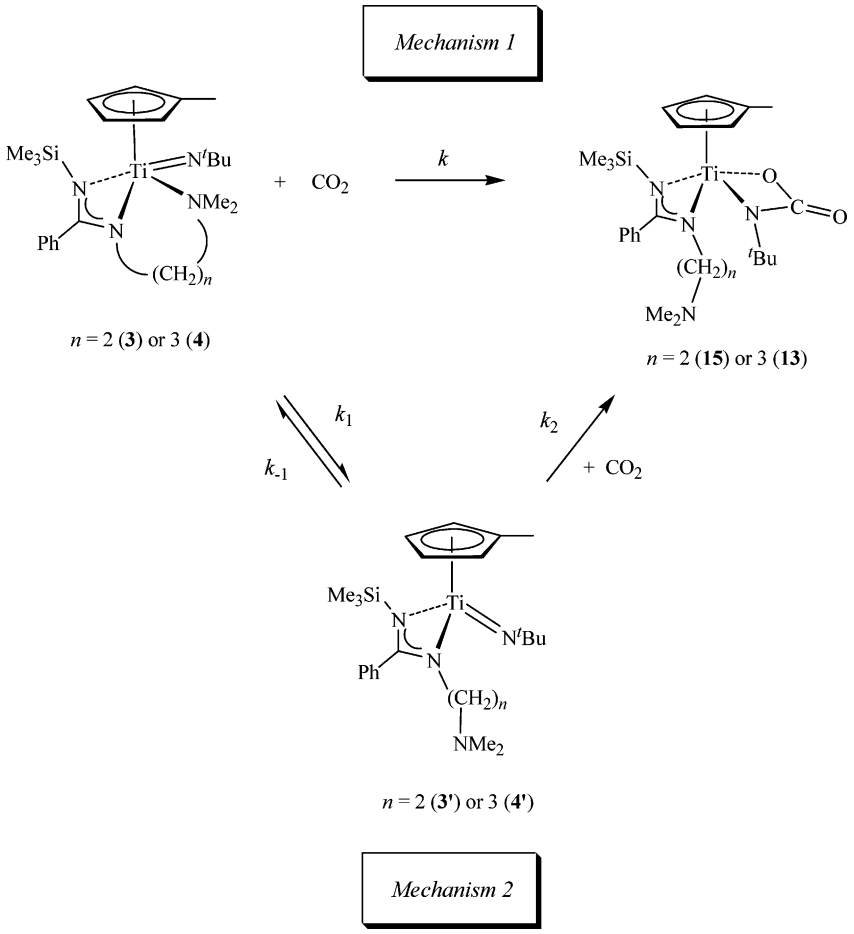

can act as spectator ligands in olefin polymerization catalysts.[64] However, the Ti=NR linkage may also promote C−H and H−H bond cleavage. Carbon−hydrogen bond activation by titanium imido complexes has been studied computationally by Cundari et al.[65] Chirik et al. have compared the C−H and H−H bond activation promoted by Ti−alkylidene and Ti−imido complexes and have related the absence of reactivity toward C−H of the latter to the respective shape of the frontier orbitals.[8] Bergman and Straub have used density functional theory calculations to elucidate the mechanism of hydroamination of allenes, alkynes, and alkenes catalyzed by cyclopentadienyl titanium imido complexes.[12] Mountford and co-workers have used density functional theory in combination with photoelectron spectroscopy to elucidate the bonding in "pogo stick" complexes of the type [Ti(η-C_8H_8)(NR)].[66] In the present work, density functional theory (DFT) calculations on model systems were performed using hybrid DFT (B3PW91).[67,68] The main objective of the theoretical study is to elucidate the potential role played by the pendant arm on the reactivity with CO_2 of the amidinate titanium imido complexes.

The reaction of the model compound [Ti(η-C_5H_5)(NMe){MeC(NMe)$_2$}] (**I**) with CO_2 was used as a reference. The global pathway for the overall reaction as summarized in eq 6 is given in Figure 6. The final

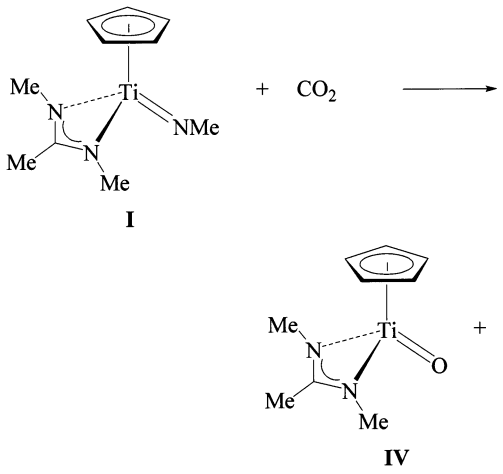

(6)

dimeric μ-oxo product [$Ti_2(\eta$-$C_5H_5)_2(\mu$-$O)_2${MeC(NMe)$_2$}$_2$] was not calculated by DFT, since this would be expensive in terms of CPU time. Furthermore, the dimerization of the terminal oxo products (as modeled by [Ti(η-C_5H_5)(O){MeC(NMe)$_2$}] (**IV**)) is not the main point of interest from an experimental or mechanistic point of view.

(64) Jensen, V. R.; Børve, K. J. *Chem. Commun.* **2002**, 542.
(65) Cundari, T. R.; Klinckman, T. R.; Wolczanski, P. T. *J. Am. Chem. Soc.* **2002**, *124*, 1481.
(66) Blake, A. J.; Cowley, A. R.; Dunn, S. C.; Green, J. C.; Hazari, N.; Jones, N. M.; Moody, A. G.; Mountford, P. *Chem. Eur. J.*, in press.
(67) Perdew, J. P.; Wang, Y. *Phys. Rev. B* **1992**, *45*, 13244.
(68) Becke, A. D. *J. Chem. Phys.* **1992**, *98*, 5648.

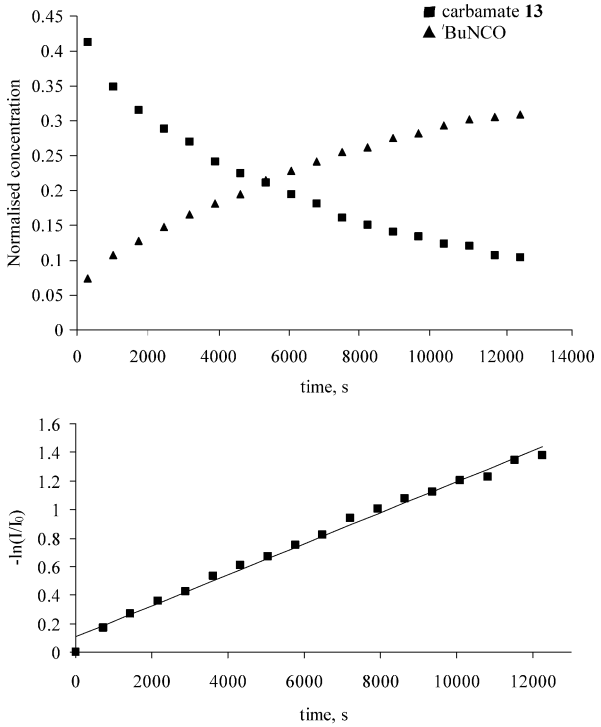

Figure 5. (a, top) Plot of normalized concentrations vs time for the ^{t}BuNCO extrusion reaction of [Ti(η-C_5H_4Me){N^{t}BuC(O)O}{$Me_3SiNC(Ph)NCH_2CH_2CH_2NMe_2$}] (**13**). Values given are for the carbamate **13** and ^{t}BuNCO. (b, bottom) Plot of ln(I/I_0) vs time for the ^{t}BuNCO extrusion reaction of [Ti(η-C_5H_4Me){N^{t}BuC(O)O}{$Me_3SiNC(Ph)NCH_2CH_2CH_2NMe_2$}] (**13**).

Table 6. First-Order Rate Constants k and Associated Half-Lives ($t_{1/2}$) for Extrusion of ^{t}BuNCO from in Situ Generated Carbamate Complexes 13−15[a]

carbamate	initial concn × 10^8 (mol dm^{-3})	$k \times 10^4$ (s^{-1})	$t_{1/2} \times 10^{-3}$ (s)
14	1.9	1.3 ± 0.03	5.63 ± 1.30
	2.9	1.2 ± 0.02	5.94 ± 0.99
	3.8	1.2 ± 0.03	6.16 ± 1.54
15	1.9	2.4 ± 0.03	2.93 ± 0.36
		2.1 ± 0.03	3.37 ± 0.48
13	1.9	1.1 ± 0.08	6.43 ± 0.55
		1.1 ± 0.02	6.30 ± 0.11

[a] Values of "initial concentration" refer to the imido precursors 3−5.

The reaction leading to the titanium terminal oxo complex **IV** and MeNCO is exothermic by 25.4 kJ mol^{-1} ($\Delta G_{\mathbf{I-IV}} = -32.2$ kJ mol^{-1}). The first step in the reaction is the side-on cycloaddition of CO_2 to the Ti=NMe bond. The direction of CO_2 attack and geometry of the transition state (**TS$_{I-II}$**) is explained by the shape of the frontier orbitals of **I** (Figure 7). The HOMO is one of the π-components of the Ti=N bond, resulting from the interaction of the titanium $3d_{yz}$ orbital with the nitrogen $2p_z$ orbital (Figure 7 gives the coordinate system), and the LUMO is essentially a $3d_{z^2}$ orbital. Consequently, the frontier orbitals of the imido group are ideally suited for efficient interaction with both the HOMO and the LUMO of CO_2, leading to a very low electronic energy activation barrier for cycloaddition of 0.6 kJ mol^{-1} ($\Delta G^{\ddagger}_{\mathbf{I-II}} = 51.7$ kJ mol^{-1}, taking into account entropy effects). The reaction proceeds exothermically to form the very stable carbamate intermediate [Ti(η-C_5H_5)-{NMeC(O)O}{$MeC(NMe)_2$}] (**II**) at −113 kJ mol^{-1} ($\Delta G_{\mathbf{I-II}} = -55.4$ kJ mol^{-1}). The very low activation energy barrier and the relatively low energy of the carbamate are in agreement with the experimental results, where cycloaddition of CO_2 to the imide to form the carbamate occurs readily, even at −78 °C for the three-carbon and "dummy" arm systems **14** and **15**.

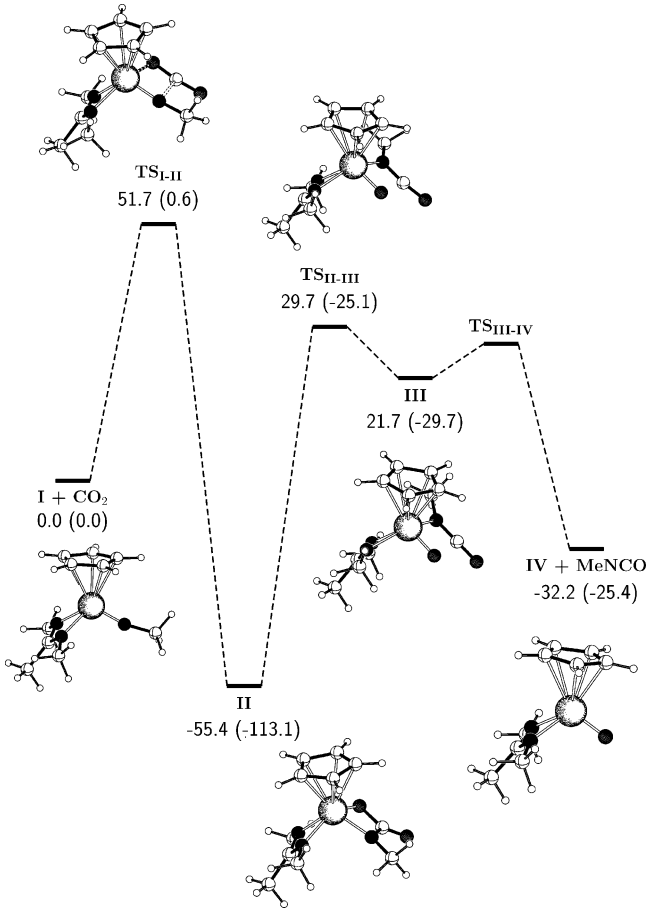

Figure 6. DFT computed pathway for the reaction of [Ti(η-C_5H_5)(NMe){$MeC(NMe)_2$}] (**I**) with CO_2 showing Gibbs free energies at 298 K (kJ mol^{-1}). Electronic energies are given in parentheses. Representations of the DFT structures are shown (left to right) for **I**, **TS$_{I-II}$**, **II**, **TS$_{II-III}$**, **III**, and **IV**. See the text for further details.

Isocyanate extrusion was found to be a two-step process. The first step is the breaking of the C−O bond of carbamate **II** to yield the isocyanate adduct [Ti(η-C_5H_5)(O)(MeNCO){$MeC(NMe)_2$}] (**III**). The activation energy barrier of 88 kJ mol^{-1} ($\Delta G^{\ddagger}_{\mathbf{II-III}} = 85.1$ kJ mol^{-1}) is associated with the concerted breaking of the C−O carbamate bond and formation of the Ti=O oxo bond (Ti−O = 1.945 Å, C−O = 1.346 Å (**II**), Ti−O = 1.666 Å, C−O = 2.222 Å (**TS$_{II-III}$**)). The second step involves crossing **TS$_{III-IV}$**, which is essentially a transition state corresponding to breaking the Ti−N bond. In the case of the symmetric system **III**, the transition state for this step has not been located but the activation barrier is likely to be no greater than ca. 10 kJ mol^{-1}, as was found to be the case for the pendant arm substituted complexes (vide infra and Table 7). Moreover, the transformation from **III** to **IV** is exothermic ($\Delta G_{\mathbf{III-IV}} = -53.9$ kJ mol^{-1}); thus, the associated TS is expected to be reactant-like and to be at low energy.

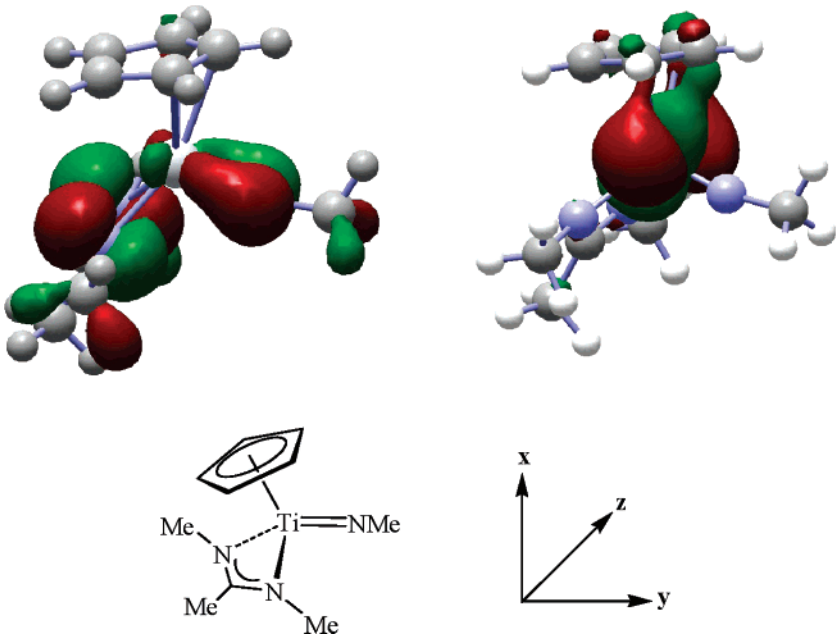

Figure 7. Representations of the HOMO (left) and LUMO (right) of the model complex **I** together with the chosen coordinate system.

Table 7. Relative Electronic Energies (kJ mol^{-1}) of Extrema along the Pathway for CO_2 Cycloaddition/MeNCO Extrusion on the Two Pendant Arm Functionalized Titanium Amidinate Complexes $\mathbf{I_{C2}}$ and $\mathbf{I_{C3}}$[a]

		$\mathbf{I_{C2}}$		$\mathbf{I_{C3}}$	
	I	SiH_3	C_2 arm	SiH_3	C_3 arm
$\mathbf{TS_{I-II}}$	0.6 (51.7)	3.5 (51.1)	4.5 (54.0)	3.0 (51.0)	4.6 (51.9)
II	−113.1 (−55.4)	−105.7 (−44.4)	−110.5 (−49.1)	−105.8 (−46.4)	−109.1 (−53.3)
$\mathbf{TS_{II-III}}$	−25.1 (29.7)	−20.6 (31.6)	−25.2 (29.7)	−21.9 (29.2)	−23.7 (25.0)
III	−29.7 (21.7)	−23.7 (27.4)	−29.4 (*25.3*)	−25.0 (*31.6*)	−27.8 (*22.3*)
$\mathbf{TS_{III-IV}}$	not located	−15.3 (30.5)	−21.4 (*19.7*)	−15.6 (*27.1*)	−20.4 (*19.5*)
IV + MeNCO	−25.4 (−32.2)	−24.6 (−33.1)	−24.6 (−33.1)	−23.7 (−33.0)	−23.7 (−33.0)

[a] Gibbs free energy values at 298 K are given in parentheses. For $\mathbf{I_{C2}}$ and $\mathbf{I_{C3}}$, SiH_3 and C_2 arm are the sides of CO_2 attack. Energies are computed with respect to the separated imido−amidinate titanium complex and CO_2. Values for the corresponding reaction of **I** and CO_2 are presented for ease of comparison.

(a) Influence of the Amidinate Pendant Arm Substituent: NMe_2 Not Chelated. The critical issue in the reactions of **3**−**5** concerns the effect of the pendant donor group (for **3** and **4**) and chain length, and whether the key Ti=N^{t}Bu/CO_2 coupling reaction takes place on a chelated (i.e., **3** or **4**) or nonchelated (**3′** or **4′**) complex. Further DFT model complexes have therefore been studied (with and without pendant group coordination). We consider first the pendant arm noncoordinated model complexes $\mathbf{I_{C2}}$ and $\mathbf{I_{C3}}$. These correspond

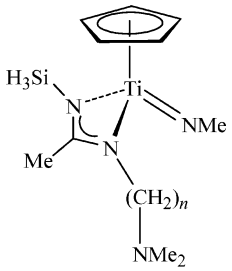

$n = 2$ ($\mathbf{I_{C2}}$) or 3 ($\mathbf{I_{C3}}$)

to the postulated intermediates in NMe_2 methyl group exchange, namely **3′** and **4′** (eq 1).

As expected, the overall pathway is analogous to that computed for **I**. However, in this case the cycloaddition of CO_2 can proceed either from the SiH_3-substituted side ($SiMe_3$ in the real compounds **3′** and **4′**), leading to the carbamate $\mathbf{II_{C2-Si}}$ or $\mathbf{II_{C3-Si}}$, or from the pendant arm side, leading to $\mathbf{II_{C2-N}}$ and $\mathbf{II_{C3-N}}$ (Figure 8). The pathways for the two regiochemistries of addition have been computed. The energies of the extrema are reported in Table 7, and the associated activation barriers for CO_2 addition and MeNCO extrusion are given in Table 8.

In terms of the energies associated with the various pathways, the identity of the noncoordinated pendant arm substituent has no significant influence. The reaction is very similar to **I** + CO_2 (Figure 6), except that in all but one case, the isocyanate adduct (for example **III** in Figure 6) is not stable enough to create a local minimum in the Gibbs free energy surface (indicated by the values given in italics in Table 7) and so extrusion could equally well be considered to be a one-step process. The difference in behavior between the energy and Gibbs free energy surfaces for the extrusion could be explained by the influence of rotational energy contributions on dissociation.

In terms of the regiochemistry, the barriers for CO_2 cycloaddition and for isocyanate extrusion are very close in energy for all four cases. For both the two-carbon and three-carbon arm systems there is a small energetic preference for CO_2 attack from the SiH_3 side to form a carbamate intermediate where the imido NMe substitu-

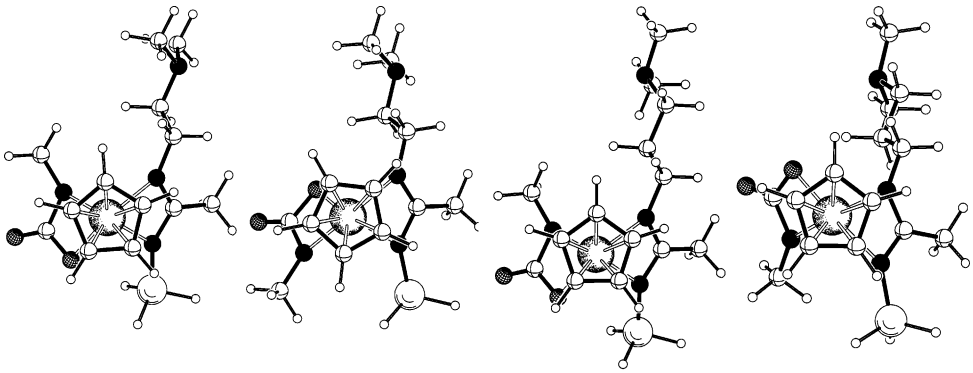

$\mathbf{II_{C2\text{-}Si}}$ $\mathbf{II_{C2\text{-}N}}$ $\mathbf{II_{C3\text{-}Si}}$ $\mathbf{II_{C3\text{-}N}}$

Figure 8. Various DFT computed carbamate complexes formed from the reaction of CO_2 with $\mathbf{I_{C2}}$ and $\mathbf{I_{C3}}$.

Table 8. Electronic Activation Energy Barriers (kJ mol^{-1}) along the Pathway for CO_2 Cycloaddition/MeNCO Extrusion Reactions of Pendant Arm Functionalized Titanium Amidinate Complexes $\mathbf{I_{C2}}$ and $\mathbf{I_{C3}}$[a]

	I_{C2}		I_{C3}	
	SiH_3	C_2 arm	SiH_3	C_3 arm
I to $\mathbf{TS_{I-II}}$	3.5 (51.1)	4.5 (54.0)	3.0 (51.0)	4.6 (51.9)
II to $\mathbf{TS_{II-III}}$	85.1 (76.0)	85.3 (78.8)	83.9 (75.6)	85.4 (78.3)

[a] Gibbs free energy values at 298 K are given in parentheses. For $\mathbf{I_{C2}}$ and $\mathbf{I_{C3}}$, SiH_3 and C_2 arm are the sides of CO_2 attack.

ent and the SiH_3 group are on opposite sides. The dissociation of MeNCO from the pendant arm side that necessarily follows CO_2 addition from the SiH_3 direction is also slightly kinetically preferred (Table 8). While these differences are not significant within the accuracy of DFT calculations, it might be expected that the small energetic preference for this regiochemistry of addition and extrusion would be increased if the actual steric bulk were to be considered (i.e. $SiMe_3$ in place of SiH_3 and ^{t}Bu in place of NMe). The crystallographically characterized carbamate complex **7** (Figure 1) formed from CO_2 and the real pentamethylcyclopentadienyl C_3 arm system **2** is consistent with CO_2 attack from the $SiMe_3$ side.

The calculations of the nonchelating model systems $\mathbf{I_{C2}}$ and $\mathbf{I_{C3}}$ imply that the CO_2 addition reactions of the real complexes **3** and **4** (and obviously **5**) would also be very similar if the pendant NMe_2 groups played only an *indirect* role. However, since the two-carbon arm system **3** does not react with CO_2 at significant rates below −35 °C and the three-carbon and "dummy-arm" homologues react rapidly even at −78 °C, it is clear that there must be a *direct* effect of the pendant NMe_2 that is different (or significantly amplified) for the two-carbon system. This will be addressed in the following section.

We turn now briefly to the isocyanate extrusion step. This occurs at the same temperature for all three of the real carbamate systems **13**−**15**, with rate constants that are very close in value. From the calculated values, the activation barrier for the isocyanate extrusion is ca. 85 kJ mol^{-1} for both the two-carbon and the three-carbon arm model systems (energy difference between **II** and $\mathbf{TS_{II-III}}$). Although the experimental results indicate that the rate of extrusion is twice as fast for the two-carbon pendant arm carbamate **15**, this translates into a $\Delta\Delta G^{\ddagger}$ value of less than 2 kJ mol^{-1}, which is below the accuracy associated with these calculations.

(b) Influence of the Amidinate Pendant Arm Substituent: NMe_2 Chelated. It is important to determine whether CO_2 cycloaddition or/and isocyanate extrusion could take place on pendant arm coordinated complexes. Model imido amidinate complexes with the pendant NMe_2 coordinated to titanium have been optimized, and the resulting geometries are shown in Figure 9(a). The chelated isomer ($\mathbf{I_{C2-chel}}$ and $\mathbf{I_{C3-chel}}$) is more stable than the nonchelated complex ($\mathbf{I_{C2}}$ and $\mathbf{I_{C3}}$) in both cases by 25.4 and 23.3 kJ mol^{-1}, respectively. In $\mathbf{I_{C3-chel}}$, the six-membered ring is in a "chair" conformation. The alternative "boat" conformation has been optimized and lies 12.2 kJ mol^{-1} higher in energy. When Gibbs free energy values are considered at 298 K, the chelated isomer $\mathbf{I_{C2-chel}}$ is still more stable than $\mathbf{I_{C2}}$, but only by 6.2 kJ mol^{-1}. For the three-carbon system, however, the nonchelated isomer $\mathbf{I_{C3-chel}}$ is now only marginally more stable (0.4 kJ mol^{-1}) than $\mathbf{I_{C3}}$. The Gibbs free energy differences between $\mathbf{I_{C2}}$ and $\mathbf{I_{C2-chel}}$ (and $\mathbf{I_{C3}}$ and $\mathbf{I_{C3-chel}}$) are lower than the electronic ΔE values, because the chelated form is entropically disfavored. Since the three-carbon chain has more rotational degrees of freedom, the impact of the decoordination upon G is more pronounced. This is in agreement with the experimental observation that NMe_2 group methyl exchange occurs at a lower temperature for the real C_3 system **14**.

Interestingly, the HOMOs for the chelated complexes (Figure 9b) are not orientated in the same plane as for the nonchelated complexes (Figure 7). For the chelated complexes the frontier orbital preferred trajectory for CO_2 addition is therefore from *below*, trans to the methylcyclopentadienyl ring. The corresponding transition states ($\mathbf{C2_{chel}TS_{I-II}}$ and $\mathbf{C3_{chel}TS_{I-II}}$) are shown in Figure 9c, and their electronic energies are 24.5 and 39.5 kJ mol^{-1}, respectively, with respect to the isolated reactants. Therefore, in terms of electronic energies, CO_2 attack on the chelated isomers $\mathbf{I_{C2-chel}}$ and $\mathbf{I_{C3-chel}}$ is disfavored by some 20−35 kJ mol^{-1} compared to attack at the nonchelated isomers $\mathbf{I_{C2}}$ and $\mathbf{I_{C3}}$. Furthermore, it is the chelated *two-carbon* arm species that should, according to the calculations, react more readily with CO_2, which is in contrast to the experimental results. Taken together, the experimental and computational data imply that preferred attack is via the nonchelated

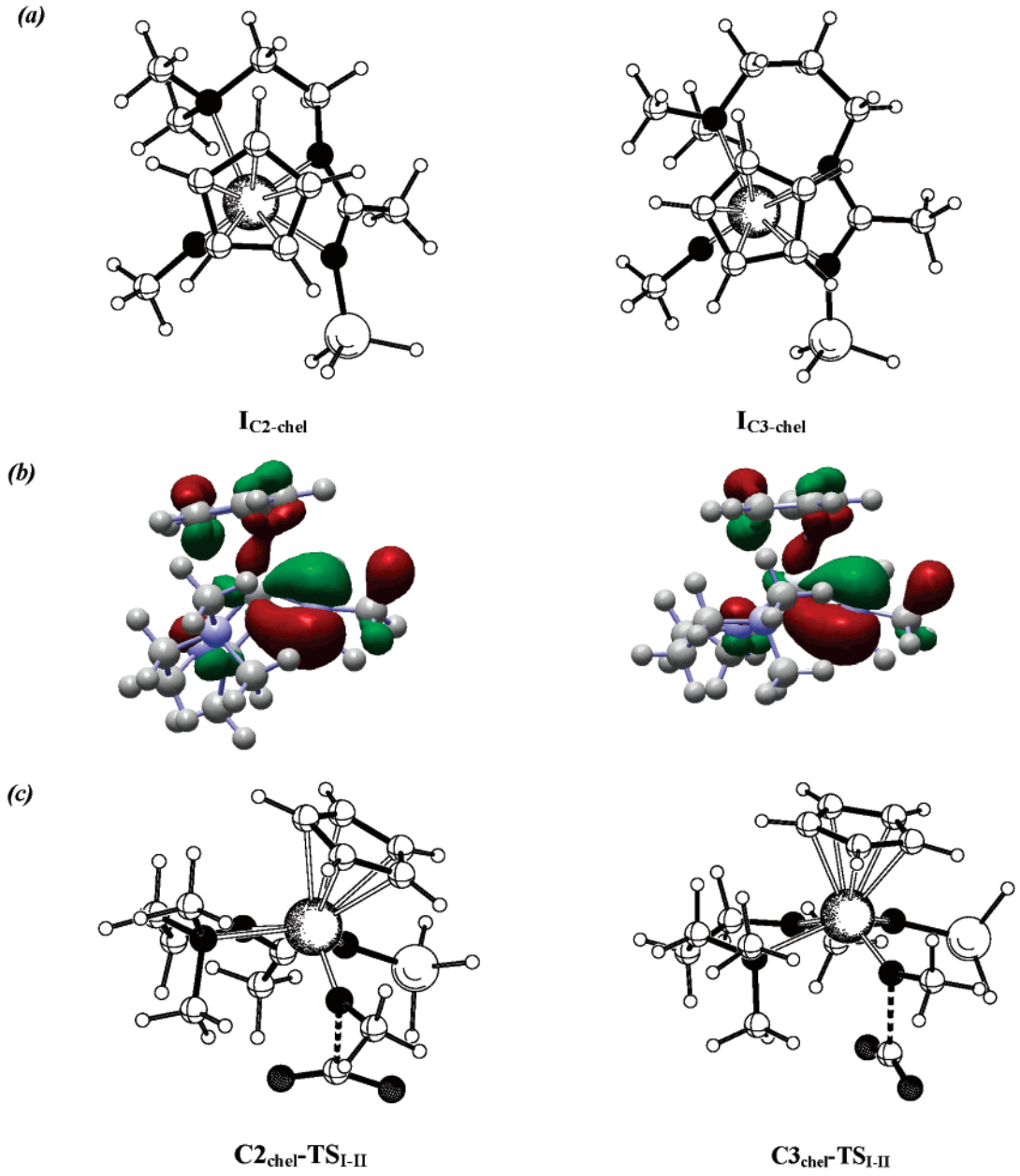

Figure 9. (a) DFT minimized geometries of the chelated imido amidinate complexes $\mathbf{I_{C2-chel}}$ (left) and $\mathbf{I_{C3-chel}}$ viewed along the $Cp_{cent}\cdots Ti$ vectors. (b) Representations of the HOMO of each compound viewed approximately perpendicular to these vectors. (c) Geometries of the transition states for CO_2 cycloaddition to Ti=NMe ($\mathbf{C2_{chel}\text{-}TS_{I-II}}$ for addition to $\mathbf{I_{C2-chel}}$ and $\mathbf{C3_{chel}\text{-}TS_{I-II}}$ for addition to $\mathbf{I_{C3-chel}}$).

isomers and that it is the activation barriers to accessing these that control the reactions.

Unfortunately, it was not possible computationally to find a transition state for dissociation of NMe_2 in the model systems (i.e. for $\mathbf{I_{C2-chel}} \rightarrow \mathbf{I_{C2}}$ or $\mathbf{I_{C3-chel}} \rightarrow \mathbf{I_{C3}}$). Such a transition state would correspond to a dissociation of NMe_2 (coupled with subsequent pendant arm chain reorganization) and would be associated with a very soft motion (low value of the imaginary frequency at the TS). Given the large number of degrees of freedom associated with the different conformations of the decoordinating $CH_2CH_2NMe_2$ and $CH_2CH_2CH_2NMe_2$ chains, it is not at all straightforward to estimate a starting geometry for the TS structure. Therefore, despite many attempts, it was not possible to locate such a transition-state structure. However, since the experimental values for NMe_2 methyl group exchange have been established (Table 1), it has been possible to make a "hybrid" comparison of computational and experimental data for the two possibilities for CO_2 attack (Figure 10). The Gibbs free energies in Figure 10 were computed for $T = 200$ K, slightly above the temperature at which the real systems **4** (three-carbon arm) and **5** ("dummy-arm") react. All energies are from DFT calculations on the species or transition states indicated, except for those for the transition state between $\mathbf{I_{C2-chel}}$ and $\mathbf{I_{C2}}$ (51.2 kJ mol^{-1}) and between $\mathbf{I_{C3-chel}}$ and $\mathbf{I_{C3}}$ (41.6 kJ mol^{-1}), which are taken from the experimental data for the real complexes **3** and **4**, respectively (Table 1)

Figure 10 unambiguously indicates that CO_2 attack would occur on the nonchelated isomers $\mathbf{I_{C2}}$ (corresponding to the real system **3′**, eq 1) and $\mathbf{I_{C3}}$ (real system **4′**). Furthermore, this preference would be reinforced as the temperature is increased (recall that **3** only reacts

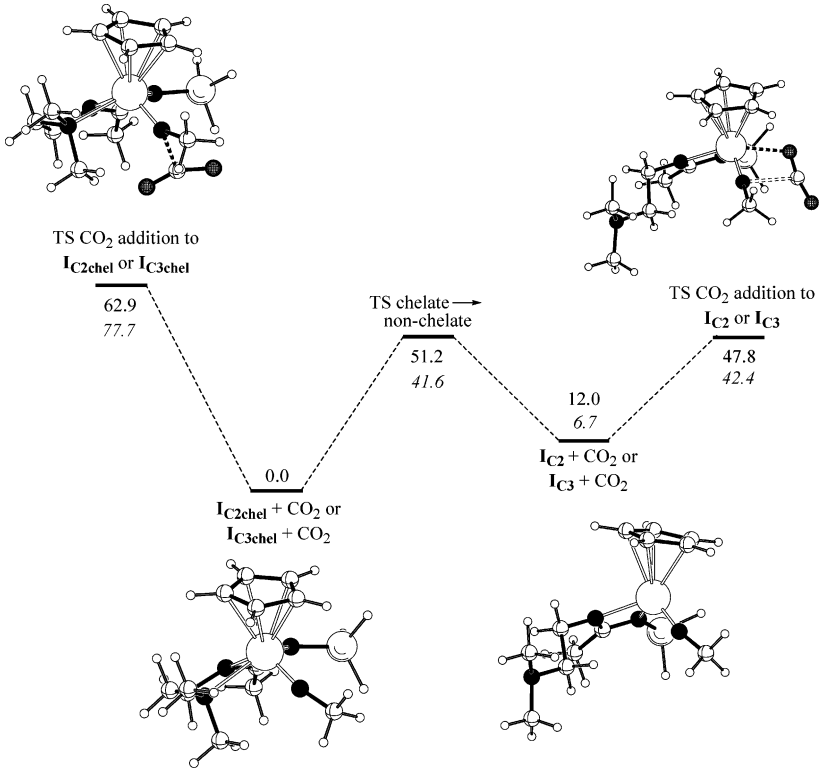

Figure 10. Schematic representation of free energies for CO_2 addition for both the chelated and nonchelated imido–amidinate systems at 200 K, relative to the respective chelated isomers. The upper value in each pair is for the two-carbon arm system and the lower value (in italics) is for the three-carbon arm systems (TS = transition state). All energies are from DFT calculations except for "TS chelate → nonchelate" which are derived from the $\Delta H^{\ddagger}$ and $\Delta S^{\ddagger}$ data for **3** and **4** (Table 1). DFT minimized geometries for the two-carbon arm system are illustrated.

at a reasonable rate above 238 K) because attack by CO_2 is entropically *disfavored* (thus the Gibbs free energy of the TS for addition to $\mathbf{I_{C2chel}}$ and $\mathbf{I_{C3chel}}$ would be *higher* than 62.9 and 77.7 kJ mol^{-1}, respectively) whereas $\Delta G^{\ddagger}$ for decoordination (leading to NMe_2 methyl exchange) is entropically *favored* and would lead to lower values than the 51.2 and 41.6 kJ mol^{-1} calculated at 200 K.

Although it is known experimentally that the real carbamate complexes **15** and **13** do not have a chelated NMe_2 group, attempts were made to elucidate computationally a mechanism for MeNCO extrusion from a carbamate complex with a chelating pendant arm. It was found that the κ^2-carbamates formed from CO_2 cycloaddition to $\mathbf{I_{C2chel}}$ or $\mathbf{I_{C3chel}}$ have to be converted to κ^1-bound carbamates before MeNCO extrusion could occur. However, it was not possible to find a transition state for this κ^2 to κ^1 interconversion which did not involve dissociation of the NMe_2 group. Therefore, not only is CO_2 attack on the chelate isomer kinetically less favored but also there is no exit channel from the κ_2-carbamate so formed, which leads to the observed products. This also further militates against the likelihood of a pendant arm anchimeric effect on extrusion of isocyanate from the carbamate complexes.

(c) Influence of Steric Factors. ONIOM calculations to take into account the influence of steric bulk have been performed. These indicate that the chelated isomer $\mathbf{I_{C2-chel}}$ is more stable than the nonchelated isomer $\mathbf{I_{C2}}$ by 3.8 kJ mol^{-1} for the C_2 system. In the case of the C_3 system, the chelated isomer $\mathbf{I_{C3-chel}}$ is slightly *less* stable than the nonchelated isomer $\mathbf{I_{C3}}$ by 4.9 kJ mol^{-1}. These values suggest that the equilibrium between the chelated and nonchelated isomers would lie in favor of the nonchelated isomer for the experimental C_3 system. This is in contrast to the clear evidence for chelation of the NMe_2 group in the low-temperature NMR spectra of this compound. Thus, while the calculated energies do not entirely reflect the experimental behavior of compound **4**, they do confirm the overall *trend* that the stabilization upon chelation is greater for the two-carbon arm system and that this trend is amplified when steric factors are considered. Again, the less favorable dissociation of the C_2 arm from titanium may account for the higher temperature required for CO_2 cycloaddition if the nonchelated isomer is the reactive species.

Conclusions

Reactions of cyclopentadienyl amidinate *tert*-butylimido complexes with CO_2 all ultimately yield oxo-bridged dimers and ^{t}BuNCO. The stabilities of the N,O-bound carbamate intermediates depend mainly on the cyclopentadienyl ring substituents, but there is also a small dependence on the nature of the length of the (dimethylamino)alkyl chain for the C_5H_4Me systems. This might be due either to small steric differences between the amidinate ligand systems or from a slight anchimeric effect of the two-carbon arm on the extrusion. The differences in the DFT calculated activation barriers for isocyanate extrusion from the two-carbon and three-carbon arm carbamate complexes without the pendant arms coordinated are too small to be significant. The origin of the small increase in the rate of isocyanate extrusion for the C_2 arm systems is therefore still somewhat unclear.

Much more pronounced are the differences in reaction temperature for onset of CO_2 cycloaddition to the Ti=N^{t}Bu bonds of **3** and **4**. The kinetics studies on the cycloaddition of CO_2 to Ti=N^{t}Bu for the two-carbon linker arm system (**3**) have established that the rate-determining step is bimolecular with a first order dependence on CO_2. In the case of the "dummy-arm" system **5**, cycloaddition necessarily occurs to a nonchelated pendant arm species. However, the first-order CO_2 dependence in the case of the pendant amine functionalized compound **3** (and probably **4**), is equally consistent with both direct cycloaddition to the coordinated isomer and pendant arm dissociation followed by cycloaddition. The DFT studies suggest that, for the three-carbon atom linker system **4**, CO_2 cycloaddition occurs to the nonchelated isomer and is essentially barrierless. This is supported by the similar behavior of **4** and the "dummy-arm" system **5**, which both undergo rapid cycloaddition of CO_2 even at −78 °C. For the two-carbon arm system **3** it is possible that CO_2 addition to the chelated isomer could be competitive, but comparison of the activation barriers for methyl group exchange (experimentally determined) and CO_2 cycloaddition (calculated) at 200 K suggest that decoordination of the pendant arm prior to CO_2 cycloaddition is energetically favored. It was not possible to optimize a transition state for NMe_2 group dissociation by DFT; thus, theoretical values are not available for comparison with the experimentally determined activation parameters. The greater energy required to decoordinate the pendant amine from titanium for the two-carbon arm system explains the higher temperature needed before CO_2 cycloaddition to **3** occurs.

The mechanistic studies of isocyanate extrusion from the "dummy-arm" system at different concentrations suggest a first-order dependence on the carbamate complex in the rate-determining step. This is consistent with extrusion to form a monomeric terminal oxo complex which then self-traps by dimerization. The flat nature of the energy profile between $\mathbf{TS_{II-III}}$ and the oxo compound **IV** suggests that there may be some reversibility in this part of the mechanism, whereby the transient terminal oxo complex can undergo back-cycloaddition of ^{t}BuNCO to re-form the carbamate intermediate unless it is trapped by dimerization. These results also suggest that it might be possible to intercept the transient Ti=O species with other unsaturated substrates.[62]

Experimental Section

General Methods and Instrumentation. All manipulations were carried out using standard Schlenk line or drybox techniques under an atmosphere of argon or of dinitrogen. Solvents were predried over 4 Å molecular sieves and were refluxed over appropriate drying agents under a dinitrogen atmosphere and collected by distillation. Deuterated solvents were dried over appropriate drying agents, distilled under reduced pressure, and stored under dinitrogen in Teflon valve ampules. NMR samples were prepared under dinitrogen in 5 mm Wilmad 507-PP tubes fitted with J. Young Teflon valves. ^{1}H, ^{13}C{^{1}H}, and ^{13}C NMR spectra were recorded on Varian Unity Plus 500 and Varian Mercury spectrometers. ^{1}H and ^{13}C assignments were confirmed where necessary with the use of NOE, DEPT-135, DEPT90, DEPT-45, and two-dimensional ^{1}H−^{1}H and ^{13}C−^{1}H NMR experiments. All spectra were referenced internally to residual protio solvent (^{1}H) or solvent (^{13}C) resonances and are reported relative to tetramethylsilane (δ 0 ppm). Chemical shifts are quoted in δ (ppm) and coupling constants in hertz. Infrared spectra were prepared as Nujol mulls or thin films between KBr or NaCl plates and were recorded on Perkin-Elmer 1600 and 1700 series spectrometers. Infrared data are quoted in wavenumbers (cm^{-1}). Mass spectra were recorded by the mass spectrometry service of the University of Oxford's Inorganic Chemistry Laboratory. Combustion analyses were recorded by the analytical services of the University of Oxford's Inorganic Chemistry Laboratory.

Literature Preparations. The compounds [Ti(η-C_5Me_5)(N^{t}Bu)Cl(py)],[52] [Ti(η-C_5H_4Me)(N^{t}Bu)Cl(py)],[52] Li[Me_3SiNC(Ph)$NCH_2CH_2NMe_2$],[47] Li[Me_3SiNC(Ph)$NCH_2CH_2CH_2NMe_2$],[48] and Li[Me_3SiNC(Ph)NCH_2CH_2Me][49] were prepared according to published methods. All other compounds and reagents were purchased and used without further purification.

Synthesis of [Ti(η-C_5Me_5)(N^{t}Bu){Me_3SiNC(Ph)$NCH_2CH_2NMe_2$}] (1). To a mixture of [Ti(η-C_5Me_5)(N^{t}Bu)Cl(py)] (1.46 g, 3.97 mmol) and Li{Me_3SiNC(Ph)$NCH_2CH_2NMe_2$} (1.07 g, 3.97 mmol) was added benzene (40 mL). The resulting dark brown solution was stirred at room temperature for 4 h and refluxed at 80 °C for 15 h; the solution became brown, and a white precipitate formed. Volatiles were removed under reduced pressure, and the resulting brown oil was extracted into benzene (40 mL). The brown solution was filtered, and volatiles were removed under reduced pressure to yield a brown oil, which was triturated with pentane (20 mL). Yield: 1.70 g (83%). The product was purified by distillation (1×10^{-5} mbar, 120−130 °C) to yield **1** as a brown waxy solid. Distilled yield: 0.25 g (45%).

^{1}H NMR data (C_6D_6, 500.1 MHz, 293 K): 7.3−7.0 (5 H, m, C_6H_5), 3.42 (1 H, m, CN_2CH_2), 3.14 (1 H, m, CN_2CH_2), 2.52 (1 H, m, C*H*$_2$NMe$_2$), 2.43 (1 H, m, C*H*$_2$NMe$_2$), 2.12 (15 H, s, C_5Me_5), 2.04 (6 H, s, NMe_2), 1.22 (9 H, s, CMe_3), −0.01 (9 H, s, $SiMe_3$). ^{13}C{^{1}H} NMR data (C_6D_6, 125.7 MHz, 293 K): 166.79 (CN_2), 135.74 (*i*-C_6H_5), 128.29, 128.11, 128.20 (5 × C of C_6H_5*), 119.26 (*C*$_5$Me$_5$), 66.89 (*C*Me$_3$), 62.30 (*C*H$_2$NMe$_2$), 46.76 (CN_2CH_2), 46.02 (NMe_2), 33.10 (C*Me*$_3$), 12.02 (C_5Me_5), 2.88 ($SiMe_3$); the asterisk indicates that other resonances were obscured by solvent. IR data (KBr plates, Nujol mull, cm^{-1}): 2766 (w), 2726 (w), 1578 (m), 1510 (s), 1485 (s, br), 1402 (s), 1348 (m), 1314 (w), 1245 (s), 1207 (w), 1189 (w), 1158 (w), 1120 (w), 1100 (w), 1057 (w, br), 1024 (m), 936 (w), 920 (m), 906 (m), 860 (w), 838 (m), 802 (w), 778 (w), 759 (w), 723 (w), 702 (w), 633 (w), 587 (w), 542 (m), 507 (w), 470 (w), 417 (w). Anal. Found (calcd for $C_{28}H_{48}N_4SiTi$): C, 65.3 (65.1); H, 9.3 (9.3); N, 10.6 (10.7).

Synthesis of [Ti(η-C_5Me_5)(N^{t}Bu){Me_3SiNC(Ph)$NCH_2CH_2CH_2NMe_2$}] (2). To a mixture of [Ti(η-C_5Me_5)(N^{t}Bu)Cl(py)] (1.25 g, 3.40 mmol) and Li{Me_3SiNC(Ph)$NCH_2CH_2CH_2NMe_2$} (0.96 g, 3.40 mmol) was added benzene (40 mL). The mixture was stirred at room temperature for 1 h and refluxed at 80 °C for 15 h, giving a cloudy red-brown solution. Volatiles were removed under reduced pressure, and the resulting red-brown oil was extracted into benzene (30 mL) and filtered. The residual solids were washed with benzene (2 × 20 mL). Volatiles were removed from the combined extracts under reduced pressure, giving a red-brown oil, which was triturated with pentane (30 mL) to yield **2** as a red-brown waxy solid. Yield: 1.61 g (89%). The product was purified by distillation (1×10^{-5} mbar, 120−130 °C) to yield **1** as a red-brown waxy solid. Distilled yield: 0.21 g (35%).

^{1}H NMR data (C_6D_6, 300.1 MHz, 293 K): 7.3−7.0 (5 H, m, C_6H_5), 3.31 (1 H, m, CN_2CH_2), 3.06 (1 H, m, CN_2CH_2), 2.18 (2 H, m, C*H*$_2$NMe$_2$), 2.15 (15 H, s, C_5Me_5), 2.08 (6 H, s, NMe_2), 1.74 (2 H, m, $CH_2CH_2CH_2$), 1.26 (9 H, s, CMe_3), 0.06 (9 H, s, $SiMe_3$). ^{13}C{^{1}H} NMR data (C_6D_6, 75.5 MHz, 293 K): 166.52 (CN_2), 135.91 (*i*-C_6H_5), 128.82, 128.30 (5 × CH of C_6H_5*), 119.21 (*C*$_5$Me$_5$), 66.92 (*C*Me$_3$), 57.55 (*C*H$_2$NMe$_2$), 46.00 (CN_2CH_2), 45.51 (NMe_2), 33.10 (C*Me*$_3$), 30.94 ($CH_2CH_2CH_2$),

12.04 (C_5Me_5), 2.96 ($SiMe_3$); the asterisk indicates that other resonances were obscured by solvent. IR data (KBr plates, Nujol mull, cm^{-1}): 2724 (m), 1612 (w), 1576 (m), 1510 (m), 1484 (s, br), 1402 (m, br), 1310 (m), 1245 (m), 1205 (w), 967 (w), 920 (w), 904 (w), 875 (w), 838 (m), 802 (w), 782 (w), 759 (w), 723 (w), 701 (w), 633 (w), 587 (w), 543 (w), 507 (w). Anal. Found (calcd for $C_{29}H_{50}N_4SiTi$): C, 65.5 (65.6); H, 9.4 (9.5); N, 10.5 (10.6).

Synthesis of [Ti(η-C_5H_4Me)(N^{t}Bu){$Me_3SiNC(Ph)NCH_2CH_2NMe_2$}] (3). To a stirred solution of [Ti(η-C_5H_4Me)(N^{t}Bu)Cl(py)] (1.81 g, 5.78 mmol) in benzene (30 mL) was added a solution of Li{$Me_3SiNC(Ph)NCH_2CH_2NMe_2$} in benzene (30 mL), dropwise over 15 min. When it was mixed, the dark brown solution turned orange and a white precipitate formed. The mixture was stirred for 15 h, volatiles were removed under reduced pressure, and the resulting red-brown oil was extracted into benzene (40 mL). The brown solution was filtered, and volatiles were removed under reduced pressure to give a red-brown oil, which was triturated with pentane (20 mL). Yield: 2.42 g (91%). The product was purified by distillation (1×10^{-5} mbar, 120−130 °C) to yield **3** as a brown oil. Distilled yield: 0.32 g (65%).

^{1}H NMR data (C_6D_6, 300.1 MHz, 293 K): 7.00−7.12 (5 H, m, C_6H_5), 6.66 (1 H, m, 3- or 4-C_5H_4Me), 6.21 (1 H, m, 4- or 3-C_5H_4Me), 5.91 (1 H, m, 2- or 5-C_5H_4Me), 5.52 (1 H, m, 5- or 2-C_5H_4Me), 2.94 (1 H, m, CN_2CH_2), 2.89 (1 H, m, CN_2CH_2), 2.34 (1 H, m, CH_2NMe_2), 2.17 (3 H, s, C_5H_4Me), 2.07 (6 H, s, NMe_2), 1.80 (1 H, m, CH_2NMe_2), 1.22 (9 H, s, CMe_3), 0.15 (9 H, s, $SiMe_3$). ^{13}C{^{1}H} NMR data (C_6D_6, 75.5 MHz, 293 K): 172.91 (CN_2), 138.46 (*i*-C_6H_5), 128.34, 128.19, 127.99, 127.80, 127.28 (5 × CH of C_6H_5), 120.28 (1-C_5H_4Me), 112.27 (2- or 5-C_5H_4Me), 110.49 (5- or 2-C_5H_4Me), 105.30 (3- or 4-C_5H_4Me), 105.01 (4- or 3-C_5H_4Me), 67.01 (CMe_3), 63.65 (CH_2NMe_2), 49.68 (NMe_2), 44.84 (CN_2CH_2), 33.46 (CMe_3), 15.17 (C_5H_4Me), 3.53 ($SiMe_3$). ^{1}H NMR data (CD_2Cl_2, 500.1 MHz, 193 K): 7.38 (3 H, m, *o*- and *p*-C_6H_5), 7.28 (2 H, m, *m*-C_6H_5), 6.34 (1H, s, 3- or 4-C_5H_4Me), 5.95 (1H, s, 4- or 3-C_5H_4Me), 5.68 (1H, s, 2- or 5-C_5H_4Me), 5.52 (1H, s, 5- or 2-C_5H_4Me), 3.16 (1H, m, CN_2CH_2), 3.09 (1H, m, CN_2CH_2), 2.63 (3H, s, NMe), 2.35 (3H, s, NMe), 2.21 (2H, m, CH_2NMe_2), 2.05 (3H, s, C_5H_4Me), 0.99 (9H, s, CMe_3), −0.19 (9H, s, $SiMe_3$). ^{13}C{^{1}H} NMR data (CD_2Cl_2, 125.7 MHz, 193 K): 173.03 (CN_2), 137.24 (*i*-C_6H_5), 128.14 (*p*-C_6H_5), 129.91 (*m*-C_6H_5), 126.91 (*o*-C_6H_5), 110.68 (2- or 5-C_5H_4Me), 107.26 (5- or 2-C_5H_4Me), 104.15 (3- and 4-C_5H_4Me, overlapping), 66.67 (CMe_3), 63.53 (CH_2NMe_2), 51.48 (NMe), 48.25 (NMe), 44.45 (CN_2CH_2), 32.50 (CMe_3), 14.74 (C_5H_4Me), 2.64 ($SiMe_3$). IR data (KBr plates, thin film, cm^{-1}): 3641 (m), 3060 (m), 2959 (s, br), 2785 (s, br), 2727 (s, br), 2648 (m), 2361(w), 2342 (w), 1952 (w), 1883 (w), 1812 (w), 1621 (w), 1602 (m), 1579 (s, br), 1402 (m), 1489 (s), 1362 (m), 1348 (m), 1331 (s), 1235 (s), 1205 (s), 1174 (w), 1159 (w), 1094 (m), 1052 (m), 1027 (s), 953 (m), 934 (w), 919 (m), 872 (s), 834 (s), 779 (s), 702 (m), 678 (m), 628 (m), 589 (w), 569 (m), 532 (w), 505 (w), 466 (w), 445 (w), 420 (w). Anal. Found (calcd for $C_{24}H_{40}N_4SiTi$): C, 62.4 (62.6); H, 8.7 (8.7); N, 12.0 (12.2).

Synthesis of [Ti(η-C_5H_4Me)(N^{t}Bu){$Me_3SiNC(Ph)NCH_2CH_2CH_2NMe_2$}] (4). To a stirred solution of [Ti(η-C_5H_4Me)(N^{t}Bu)Cl(py)] (1.04 g, 3.33 mmol) in benzene (30 mL) was added a solution of Li{$Me_3SiNC(Ph)NCH_2CH_2CH_2NMe_2$} (0.94 g, 3.33 mmol) in benzene (30 mL), dropwise over 15 min. The brown mixture was stirred for 15 h. Volatiles were removed under reduced pressure, and the resulting brown oil was extracted into benzene (30 mL) and the extract filtered. Volatiles were removed under reduced pressure, and the solid brown residues were washed with benzene (2 × 20 mL). Volatiles were removed from the combined extracts under reduced pressure to give a dark brown oil. Yield: 1.33 g (84%). The product was distilled under high vacuum (1×10^{-5} mbar, 120−130 °C) to yield **4** as a brown oil. Yield: 1.21 g (79%).

^{1}H NMR data (C_6D_6, 500.1 MHz, 293 K): 7.2−7.0 (5 H, m, C_6H_5), 6.81 (1 H, m, 3- or 4-C_5H_4Me), 6.57 (1 H, m, 4- or 3-C_5H_4Me), 5.87 (1 H, m, 2- or 5-C_5H_4Me), 5.72 (1 H, m, 5- or 2-C_5H_4Me), 3.20 (1 H, m, CN_2CH_2), 2.81 (1 H, m, CN_2CH_2), 2.29 (1 H, m, CH_2NMe_2), 2.17 (6 H, s, NMe_2), 2.04 (3 H, s, C_5H_4Me), 1.95 (1 H, m, CH_2NMe_2), 1.60 (1 H, m, $CH_2CH_2CH_2$), 1.28 (9 H, s, CMe_3), 1.23 (1 H, m, $CH_2CH_2CH_2$), 0.08 (9 H, s, $SiMe_3$). ^{13}C{^{1}H} NMR data (C_6D_6, 125.7 MHz, 293 K): 169.39 (CN_2), 137.12 (*i*-C_6H_5), 128.35, 128.30, 127.47 (5 × CH of C_6H_5*), 121.20 (1-C_5H_4Me), 113.27 (2- or 5-C_5H_4Me), 111.40 (5- or 2-C_5H_4Me), 106.53 (3- or 4-C_5H_4Me), 106.42 (4- or 3-C_5H_4Me), 67.38 (CMe_3), 60.02 (CH_2NMe_2), 48.96 (NMe_2), 46.27 (CN_2CH_2), 33.31 (CMe_3), 28.26 ($CH_2CH_2CH_2$), 14.84 (C_5H_4Me), 2.95 ($SiMe_3$); the asterisk indicates that other resonances were obscured by solvent resonance. ^{1}H NMR data (CD_2Cl_2, 500.1 MHz, 193 K): 7.38 (1 H, m, *p*-C_6H_5), 7.31 (2 H, m, *m*-C_6H_5), 7.21−7.06 (2 H, m, *o*-C_6H_5), 6.32 (1 H, m, 3- or 4-C_5H_4Me), 6.13 (1 H, m, 3- or 4- C_5H_4Me), 5.48 (1 H, m, 2- or 5- C_5H_4Me), 5.44 (1 H, m, 5- or 2-C_5H_4Me), 2.74 (1 H, m, CN_2CH_2), 2.74 (1 H, m, CH_2NMe_2), 2.57 (1 H, m, CN_2CH_2), 2.57 (3 H, s, NMe), 2.43 (3 H, s, NMe), 2.07 (1 H, m, CH_2NMe_2), 1.89 (3 H, s, C_5H_4Me), 1.83 (1 H, m, $CH_2CH_2CH_2$), 1.23 (1 H, m, $CH_2CH_2CH_2$), 0.99 (9H, s, CMe_3), −0.31 (9 H, s, $SiMe_3$). ^{13}C{^{1}H} NMR data (CD_2Cl_2, 125.7 MHz, 193 K): 171.42 (CN_2), 136.87 (*i*-C_6H_5), 127.62 (*p*-C_6H_5), 127.05 (*m*-C_6H_5), 126.51 (*o*-C_6H_5), 125.52 (*o*-C_6H_5), 117.42 (1-C_5H_4Me), 113.16 (2- or 5-C_5H_4Me), 110.37 (5- or 2-C_5H_4Me), 102.34 (3- or 4-C_5H_4Me), 101.06 (4- or 3-C_5H_4Me), 66.84 (CMe_3), 61.39 (CH_2NMe_2), 53.57 (NMe), 53.36 (NMe), 44.00 (CN_2CH_2), 32.29 (CMe_3), 24.44 ($CH_2CH_2CH_2$), 13.67 (C_5H_4Me), 1.85 ($SiMe_3$). IR data (KBr plates, thin film, cm^{-1}): 3050 (m), 2856 (s), 2824 (s, br), 2766 (s), 1422 (s, br), 1348 (s), 1298 (s), 1226 (s), 1200 (s), 1112 (m), 1098 (m), 1072 (m), 1018 (m), 980 (m), 944 (m), 898 (m, br), 836 (m, br), 782 (m), 758 (w), 700 (w), 678 (w), 626 (w), 548 (w), 530 (w), 508 (w). EI-MS: *m/z* 279 [$Me_3SiNC(Ph)NCH_2CH_2CH_2NMe_2$]$^+$ 13%, 58 [$CHMe_3$]$^+$ 100%. Anal. Found (calcd for $C_{25}H_{42}N_4SiTi$): C, 62.7 (63.2); H, 8.8 (8.9); N, 11.4 (11.8).

Synthesis of [Ti(η-C_5H_4Me)(N^{t}Bu){$Me_3SiNC(Ph)NCH_2CH_2Me$}] (5). To a stirred solution of [Ti(η-C_5H_4Me)(N^{t}Bu)Cl(py)] (1.53 g, 4.90 mmol) in benzene (30 mL) was added a solution of [Li_2{$Me_3NSiNC(Ph)NCH_2CH_2Me$}$_2$(Et_2O)$_2$] (1.54 g, 4.90 mmol) in benzene (30 mL). The deep red solution became slightly lighter in color and was stirred for 15 h. Volatiles were removed under reduced pressure, and the red oily residue was extracted into benzene (30 mL), the extract was filtered, and the volatiles were evaporated to yield **5** as a red oil. Yield: 1.96 g (94%).

^{1}H NMR data (C_6D_6, 500.1 MHz, 293 K): 7.16 (2H, m, *o*-C_6H_5), 7.05−7.10 (3H, m, *m*- and *p*-C_6H_5), 6.83 (2H, m, 3- and 4-C_5H_4Me), 5.83 (2H, m, 2- and 5-C_5H_4Me), 3.12 (1H, m, CN_2CH_2), 2.81 (1H, m, CN_2CH_2), 1.98 (3H, s, C_5H_4Me), 1.33 (2H, m, CH_2CH_3), 1.19 (9H, s, CMe_3), 0.80 (3H, t, CH_2CH_3), −0.05 (9H, s, $SiMe_3$). ^{13}C{^{1}H} NMR data (C_6D_6, 125.5 MHz, 293 K): 165.24 (CN_2), 135.94 (*i*-C_6H_5), 128.68 (*m*- or *p*-C_6H_5), 128.49 (*p*- or *m*-C_6H_5), 127.78 (*o*-C_6H_5), 113.29 (2- or 5-C_5H_4Me), 112.19 (2- or 5-C_5H_4Me), 109.14 (3- or 4-C_5H_4Me), 108.98 (3- or 4-C_5H_4Me), 67.46 (CMe_3), 51.72 (CN_2CH_2), 33.51 (CMe_3), 26.52 (CH_2CH_3), 15.44 (C_5H_4Me), 13.13 (CH_2CH_3), 3.24 ($SiMe_3$). ^{1}H NMR data (CD_2Cl_2, 500.1 MHz, 195 K): 7.29−7.45 (3H, m, br, *o*- and *m*-C_6H_5), 7.12 (1H, m, *p*-C_6H_5), 6.92 (2H, s, 3- and 4-C_5H_4Me), 5.59 (1H, s, 5- or 2-C_5H_4Me), 5.55 (1H, s, 2- or 5-C_5H_4Me), 3.02 (1H, m, CN_2CH_2), 2.77 (1H, m, CN_2CH_2), 1.81 (3H, s, C_5H_4Me), 1.22 (2H, m, CH_2CH_3), 0.89 (CMe_3), 0.77 (CH_2CH_3), −0.35 ($SiMe_3$). IR data (KBr plates, thin film, cm^{-1}): 3024 (m), 2932 (s), 2893 (s), 2854 (s), 1602 (w), 1578 (w), 1510 (s), 1480 (s), 1414 (s), 1376 (m), 1348 (s), 1292 (m), 1244 (s), 1206 (m), 1156 (w), 1120 (m), 1072 (s), 1016 (m), 922 (s), 878 (m), 836 (s), 804 (m), 782 (s), 758 (m), 686 (m), 632 (m), 594 (m), 426 (m), 412 (m). High-resolution EI-MS, found (calcd for $C_{23}H_{37}N_3SiTi$): *m/z* 431.2227 (431.2236). Anal. Found (calcd for $C_{23}H_{37}N_3SiTi$): C, 62.9 (64.0); H, 8.4 (8.6); N, 9.8 (9.7).

Synthesis of [Ti(η-C_5Me_5){$OC(O)N^tBu$}{$Me_3SiNC(Ph)NCH_2CH_2NMe_2$}] (6). A solution of [Ti(η-C_5Me_5)(N^{t}Bu)-

{$Me_3SiNC(Ph)NCH_2CH_2NMe_2$}] (**1**; 106 mg, 20.6 mmol) in pentane (10 mL) was exposed to ca. 1 atm of CO_2 via a dual-manifold Schlenk line. The solution was stirred and volatiles removed under reduced pressure as soon as the brown solution became cherry red (ca. 5 min). The resulting red powder was stored at −30 °C in a drybox. Yield: 87 mg (76%).

^{1}H NMR data (C_6D_6, 500.1 MHz, 293 K): 7.0−6.9 (5 H, m, C_6H_5), 3.56 (2 H, m, CN_2CH_2), 2.38 (1 H, m, CH_2NMe$_2$), 2.10 (1 H, m, CH_2NMe$_2$), 1.99 (15 H, s, C_5Me_5), 1.84 (6 H, s, NMe_2), 1.48 (9 H, s, CMe_3), −0.05 (9 H, s, $SiMe_3$). ^{13}C{^{1}H} NMR data (C_6D_6, 125.7 MHz, 293 K): 175.75 (N*C*(O)O), 158.88 (*C*N_2), 135.11 (*i*-C_6H_5), 129.17 (C_6H_5), 128.80 (*C*$_5$Me$_5$), 128.49, 128.37, 127.45, 126.92 (4 × CH of C_6H_5), 60.51 (*C*H$_2$NMe$_2$), 57.76 (*C*Me$_3$), 48.22 (CN_2*C*H$_2$), 45.50 (NMe_2), 31.30 (C*Me*$_3$), 12.69 (C_5*Me*$_5$), 2.34 ($SiMe_3$). IR data (KBr plates, Nujol mull, cm^{-1}): 2726 (m), 2670 (w), 1686 (m), 1304 (m, br), 1260 (m, br), 1246 (m), 1156 (m, br), 1024 (m), 918 (m), 892 (m), 840 (m), 722 (s), 688 (s). Anal. Found (calcd): C, 59.9 (62.1); H, 8.0 (8.6); N, 9.8 (10.0).

Synthesis of [Ti(η-C$_5$Me$_5$){OC(O)N^{t}Bu}{Me$_3$SiNC(Ph)NCH$_2$CH$_2$CH$_2$NMe$_2$}] (7). A solution of [Ti(η-C_5H_5)(N^{t}Bu){$Me_3SiNC(Ph)NCH_2CH_2CH_2NMe_2$}] (**2**; 100 mg, 18.9 mmol) in pentane (10 mL) was exposed to ca. 1 atm of CO_2 via a dual-manifold Schlenk line. The solution was stirred, and volatiles were removed under reduced pressure as soon as the brown solution became cherry red (ca. 5 min). The resulting red powder was stored at −30 °C in a drybox. Yield: 90 mg (82%).

^{1}H NMR data (C_6D_6, 500.1 MHz, 293 K): 7.0−6.9 (5 H, m, C_6H_5), 3.42 (2 H, m, CH_2C*H*$_2$CH$_2$), 1.96 (15 H, s, C_5Me_5), 1.81 (6 H, s, NMe_2), 1.75 (2 H, m, C*H*$_2$NMe$_2$), 1.61 (2 H, m, CN_2CH_2), 1.49 (9 H, s, C*Me*$_3$), −0.05 (9 H, s, $SiMe_3$). ^{13}C{^{1}H} NMR data (C_6D_6, 125.7 MHz, 293 K): 175.31 (N*C*(O)O), 159.13 (*C*N_2), 135.25 (*i*-C_6H_5), 129.12 (C_6H_5), 128.74 (*C*$_5$Me$_5$), 128.59, 128.51, 128.27, 126.85 (4 × CH of *C*$_6$H$_5$), 58.15 (*C*H$_2$NMe$_2$), 57.66 (C*Me*$_3$), 48.17 (CH_2*C*H$_2$CH$_2$), 45.30 (NMe_2), 31.17 (C*Me*$_3$), 30.24 (CN_2*C*H$_2$), 12.71 (C_5*Me*$_5$), 2.36 ($SiMe_3$). IR data (KBr plates, Nujol mull, cm^{-1}): 2762 (w), 2722 (w), 2670 (w), 1666 (s, br), 1514 (m), 1356 (m), 1306 (w), 1246 (m), 1180 (w), 1158 (w), 1058 (w), 1024 (w), 1010 (w), 936 (m), 918 (w), 886 (m), 874 (m), 840 (w), 794 (w), 778 (w), 756 (w), 722 (m). Anal. Found (calcd): C, 61.6 (62.7); H, 9.2 (8.8); N, 9.5 (9.8).

Synthesis of [Ti$_2$(η-C$_5$Me$_5$)$_2$(μ-O)$_2${Me$_3$SiNC(Ph)NCH$_2$CH$_2$NMe$_2$}$_2$] (8). A solution of [Ti(η-C_5Me_5)(N^{t}Bu){$Me_3SiNC(Ph)NCH_2CH_2NMe_2$}] (**1**; 0.18 g, 0.35 mmol) in benzene (15 mL) was exposed to ca. 1 atm of CO_2 via a dual-manifold Schlenk line. The solution was stirred and left to stand at room temperature for 4 days, during which time the brown solution became red-brown and some precipitation of brown powder was observed. Volatiles were removed under reduced pressure to give **8** as a red-brown waxy solid. Yield: 0.13 g (74%).

Too insoluble to obtain NMR data. IR data (KBr plates, Nujol mull, cm^{-1}): 2207 (w), 1691 (w), 1559 (w), 1521 (w), 1246 (s), 1187 (w), 1156 (w), 1097(m), 1023 (m), 964 (m), 899 (s, br), 838 (s, br), 799 (w), 750 (w), 722 (m), 701 (w), 638 (w), 610 (w), 596 (w), 503 (w), 468 (w). Anal. Found (calcd for $C_{48}H_{78}N_6O_2Si_2Ti_2$): C, 55.7 (68.0); H, 9.4 (9.3); N, 8.3 (9.9).

Synthesis of [Ti$_2$(η-C$_5$Me$_5$)$_2$(μ-O)$_2${Me$_3$SiNC(Ph)NCH$_2$CH$_2$CH$_2$NMe$_2$}$_2$] (9). A solution of [Ti(η-C_5Me_5)(N^{t}Bu){$Me_3SiNC(Ph)NCH_2CH_2CH_2NMe_2$}] (**2**; 234 mg, 0.44 mmol) in 15 mL of benzene was exposed to ca. 1 atm of CO_2 via a dual-manifold Schlenk line. The solution was stirred and left to stand at room temperature for 4 days, after which it turned brown and some precipitation of brown powder was observed. Volatiles were removed under reduced pressure to give **9** as a brown waxy solid. Yield: 0.13 g (64%).

Too insoluble for NMR data. IR data (KBr plates, Nujol mull, cm^{-1}): 1603 (m), 1532 (m), 1311 (m), 1261 (s), 1247 (s), 1155 (s, br), 1094 (s, br), 1010 (s, br), 981 (m), 912 (s), 839 (s), 723 (m), 701 (m), 630 (w), 609 (w), 475 (w). EI-MS: *m/z* 936 [M − Me]$^+$ 29%. Anal. Found (calcd for $C_{50}H_{82}N_6O_2Si_2Ti_2$): C, 60.2 (63.1); H, 8.3 (8.7); N, 8.1 (8.8).

Synthesis of [Ti$_2$(η-C$_5$H$_4$Me)$_2$(μ-O)$_2${Me$_3$SiNC(Ph)NCH$_2$CH$_2$NMe$_2$}$_2$] (10). A solution of [Ti(η-C_5H_4Me)(N^{t}Bu){$Me_3SiNC(Ph)NCH_2CH_2NMe_2$}] (**3**; 0.40 g, 0.86 mmol) in benzene (15 mL) was exposed to ca. 1 atm of CO_2 via a dual-manifold Schlenk line. The solution immediately changed color from red-brown to cherry red and after 24 h turned brown. Volatiles were removed under reduced pressure, giving a brown oil, which was triturated with pentane (20 mL) to give a waxy brown solid that was shown by NMR to be a mixture of two isomers, **10a** and **10b**. Yield: 0.19 g (56%). A sample of the crude product (0.16 g, 0.35 mmol) was recrystallized from a mixture of CH_2Cl_2 (10 mL) and hexanes (20 mL) to yield analytically pure product. Yield: 6.6 mg (5%).

IR data (KBr plates, Nujol mull, cm^{-1}): 1516 (w), 1488 (s), 1350 (m), 1304 (w, br), 1246 (m), 1204 (w), 1198 (w), 1154 (w), 1098 (w), 1024 (m), 938 (m), 918 (m), 900 (m, br), 862 (m), 836 (m), 796 (w), 722 (m, br), 700 (w), 680 (w). Anal. Found (calcd for $C_{40}H_{62}N_6O_2Si_2Ti_2$): C, 59.1 (59.2); H, 7.6 (7.7); N, 10.6 (10.4).

^{1}H NMR data for **10a** (C_6D_6, 500.1 MHz, 293 K): 7.03−7.14 (10 H, m, C_6H_5), 6.63 (2 H, m, 3- or 4-C_5H_4Me), 6.59 (2 H, m, 4- or 3-C_5H_4Me), 6.30 (2 H, m, 2- or 5-C_5H_4Me), 6.24 (2 H, m, 5- or 2-C_5H_4Me), 3.34 (2 H, m, CN_2CH_2), 3.17 (2 H, m, CN_2CH_2), 2.65 (2 H, m, C*H*$_2$NMe$_2$), 2.33 (2 H, m, C*H*$_2$NMe$_2$), 2.04 (6 H, s, C_5H_4*Me*), 0.11 (18 H, s, $SiMe_3$). ^{13}C{^{1}H} NMR data for **10a** (C_6D_6, 125.7 MHz, 293 K): 173.93 (CN_2), 136.54 (*i*-C_6H_5), 128.68, 128.42, 128.29, 127.00, 126.96 (5 × CH of C_6H_5), 114.25 (2- or 5-*C*$_5$H$_4$Me), 113.0−113.1 (3- and 4-*C*$_5$H$_4$Me), 112.18 (5- or 2-*C*$_5$H$_4$Me), 60.90 (*C*H$_2$NMe$_2$), 60.89 (*C*Me$_3$), 47.00 (CN_2*C*H$_2$), 45.89 (C_5H_4*Me*), 15.75 (NMe), 2.84 ($SiMe_3$), 1-C_5H_4Me not observed. ^{1}H NMR data (CD_2Cl_2, 500.1 MHz, 293 K): 7.48−7.39 (10H, m, br, C_6H_5), 6.30 (2H, m, 3- or 4-C_5H_4Me), 6.25 (4- or 3-C_5H_4Me), 6.04 (2H, m, 2-or 5-C_5H_4Me), 6.01 (2H, m, 5- or 2-C_5H_4Me), 3.14 (2H, m, CN_2CH_2), 3.00 (2H, m, CN_2CH_2), 2.43 (2H, m, C*H*$_2$NMe$_2$), 2.27 (2H, m, C*H*$_2$NMe$_2$), 2.21 (6H, s, C_5H_4*Me*), 2.02 (12H, s, NMe_2), −0.11 (18H, s, $SiMe_3$).

^{1}H NMR data for **10b** (C_6D_6, 500.1 MHz, 293 K): 7.03−7.14 (10 H, m, C_6H_5), 6.63 (2 H, m, 3- or 4-C_5H_4Me), 6.59 (2 H, m, 4- or 3-C_5H_4Me), 6.30 (2 H, m, 2- or 5-C_5H_4Me), 6.24 (2 H, m, 5- or 2-C_5H_4Me), 3.34 (2 H, m, CN_2CH_2), 3.17 (2 H, m, CN_2CH_2), 2.65 (2 H, m, C*H*$_2$NMe$_2$), 2.33 (2 H, m, C*H*$_2$NMe$_2$), 2.01 (6 H, s, C_5H_4*Me*), 0.88 (18 H, s, $SiMe_3$). ^{13}C{^{1}H} NMR data for **10b** (C_6D_6, 125.7 MHz, 293 K): 173.82 (*C*N_2), 136.45 (*i*-C_6H_5), 128.64, 128.44, 127.91, 127.00, 126.84 (5 × CH of *C*$_6$H$_5$), 114.12 (2- or 5-*C*$_5$H$_4$Me), 113.0−113.1 (3- and 4-*C*$_5$H$_4$Me), 112.50 (5- or 2-*C*$_5$H$_4$Me), 60.90 (*C*H$_2$NMe$_2$), 60.89 (*C*Me$_3$), 47.00 (CN_2*C*H$_2$), 45.84 (C_5H_4*Me*), 15.75 (NMe), 2.79 ($SiMe_3$). 1-C_5H_4Me not observed. ^{1}H NMR data for **10b** (CD_2Cl_2, 500.1 MHz, 293 K): 7.48−7.39 (10H, m, br, C_6H_5), 6.30 (2H, m, 3- or 4-C_5H_4Me), 6.25 (4- or 3-C_5H_4Me), 6.04 (2H, m, 2-or 5-C_5H_4Me), 6.01 (2H, m, 5- or 2-C_5H_4Me), 3.14 (2H, m, CN_2CH_2), 3.00 (2H, m, CN_2CH_2), 2.43 (2H, m, C*H*$_2$NMe$_2$), 2.27 (2H, m, C*H*$_2$NMe$_2$), 2.23 (6H, s, C_5H_4*Me*), 2.03 (12H, s, NMe_2), −0.15 (18H, s, $SiMe_3$).

Synthesis of [Ti$_2$(η-C$_5$H$_4$Me)$_2$(μ-O)$_2${Me$_3$SiNC(Ph)NCH$_2$CH$_2$CH$_2$NMe$_2$}$_2$] (11). A solution of [Ti(η-C_5H_4Me)(N^{t}Bu){$Me_3SiNC(Ph)NCH_2CH_2CH_2NMe_2$}] (**4**) in benzene (150 mg, 0.32 mmol) was exposed to ca. 1 atm of CO_2 via a dual-manifold Schlenk line. The solution was stirred and immediately changed color from red-brown to cherry red; after 5 days the solution was brown and some precipitation of brown powder was observed. Benzene was removed under reduced pressure to give a red-brown solid which was shown by NMR to be a mixture of two isomers, **11a** and **11b**. Attempts to recrystallize a portion of this product from a mixture of CH_2Cl_2 and hexanes failed to yield an analytically pure sample. Yield: 70 mg (50%).

IR data (KBr plates, Nujol mull, cm^{-1}): 1515 (s), 1309 (m), 1261 (s), 1203 (m), 1154 (w), 1090 (w), 1024 (w), 964 (m), 919 (m), 902 (m), 871 (w), 839 (s), 798 (s), 752 (w), 723 (m), 701 (m), 509 (m). Anal. Found (calcd for $C_{42}H_{66}N_6O_2Si_2Ti_2$): C, 58.9 (60.1); H, 7.8 (7.9); N, 10.1 (10.0).

^{1}H NMR data for **11a** (C_6D_6, 500.1 MHz, 293 K): 7.03−7.22 (10 H, m, C_6H_5), 6.61 (2 H, m, 3- or 4- C_5H_4Me), 6.55 (2 H, m, 4- or 3-C_5H_4Me), 6.28 (2 H, m, 2- or 5-C_5H_4Me), 6.24 (2 H, m, 5- or 2-C_5H_4Me), 3.25 (2 H, m, CN_2CH_2), 3.05 (2 H, m, CN_2CH_2), 2.36 (6 H, s, C_5H_4*Me*), 2.05 (6 H, s, NMe), 2.00 (4 H, m, C*H*$_2$NMe$_2$), 1.67 (2 H, m, $CH_2CH_2CH_2$), 1.42 (2 H, m, $CH_2CH_2CH_2$), 0.15 (18 H, s, $SiMe_3$). ^{13}C{^{1}H} NMR data for **11a** (C_6D_6, 125.7 MHz, 293 K): 173.54 (*C*N_2), 136.62 (*i*-C_6H_5 or *i*-C_5H_4Me), 128.48, 128.10, 127.91, 126.93, 126.91 (5 × CH of C_6H_5), 124.68 (1-*C*$_5$H$_4$Me), 113.99 (2- or 5-*C*$_5$H$_4$Me), 113.02 (3- and 4-*C*$_5$H$_4$Me), 112.40 (5- or 2-*C*$_5$H$_4$Me), 57.82 (*C*H$_2$NMe$_2$), 55.12 (*C*Me$_3$), 47.08 (CN_2CH_2), 45.50 (NMe), 31.46 ($CH_2CH_2CH_2$), 15.79 (C_5H_4*Me*), 2.84 ($SiMe_3$). ^{1}H NMR data for **11a** (CD_2Cl_2, 500.1 MHz, 293 K): 7.12−7.50 (10 H, m, br, C_6H_5), 6.28 (2 H, m, 3- or 4-C_5H_4Me), 6.21 (2 H, m, 4- or 3-C_5H_4Me), 6.04 (4 H, m, 2- and 5-C_5H_4Me), 2.7−3.2 (4 H, m, CN_2CH_2), 2.27 (6 H, s, C_5H_4*Me*), 2.04 (12 H, s, NMe_2), 2.00 (4 H, m, CH_2NMe_2, overlapping), 1.60 (2 H, m, $CH_2CH_2CH_2$), −0.10 (18 H, s, $SiMe_3$).

^{1}H NMR data for **11b** (C_6D_6, 500.1 MHz, 293 K): 7.0−7.1 (10 H, m, C_6H_5), 6.61 (2 H, m, 3- or 4-C_5H_4Me), 6.55 (2 H, m, 4- or 3-C_5H_4Me), 6.28 (2 H, m, 2- or 5-C_5H_4Me), 6.24 (2 H, m, 5- or 2-C_5H_4Me), 3.25 (2 H, m, CN_2CH_2), 3.05 (2H, m, CN_2CH_2), 2.35 (6 H, s, C_5H_4*Me*), 2.06 (6 H, s, NMe), 2.05 (4 H, m, C*H*$_2$NMe$_2$), 1.67 (2 H, m, $CH_2CH_2CH_2$), 1.42 (2 H, m, $CH_2CH_2CH_2$), 0.12 (18 H, s, $SiMe_3$). ^{13}C{^{1}H} NMR data for **11b** (C_6D_6, 125.7 MHz, 289 K): 173.62 (*C*N_2), 136.62 (*i*-C_6H_5 or *i*-C_5H_4Me), 128.61, 128.10, 127.91, 126.87 (5 × CH of *C*$_6$H$_5$), 124.68 (1-*C*$_5$H$_4$Me), 114.52 (2- or 5-*C*$_5$H$_4$Me), 113.02 (3- and 4-*C*$_5$H$_4$Me), 112.02 (5- or 2-*C*$_6$H$_4$Me), 57.82 (*C*H$_2$NMe$_2$), 55.12 (*C*Me$_3$), 47.08 (CN_2CH_2), 45.49 (NMe), 31.44 ($CH_2CH_2CH_2$), 15.79 (C_5H_4*Me*), 2.79 ($SiMe_3$), 1 × C_6H_5 obscured by solvent. ^{1}H NMR data for **11b** (CD_2Cl_2, 500.1 MHz, 293 K): 7.12−7.50 (10 H, m, br, C_6H_5), 6.45 (2 H, m, 3- or 4-C_5H_4Me), 6.37 (2 H, m, 4- or 3-C_5H_4Me), 6.04 (4 H, m, 2- and 5-C_5H_4Me), 2.7−3.2 (4 H, m, CN_2CH_2), 2.22 (6 H, s, C_5H_4*Me*), 2.01 (12 H, s, NMe_2), 2.00 (4 H, m, C*H*$_2$NMe$_2$, overlapping), 1.60 (2 H, m, $CH_2CH_2CH_2$), 1.35 (2 H, m, $CH_2CH_2CH_2$), −0.12 (18 H, s, $SiMe_3$).

Synthesis of [Ti$_2$(η-C$_5$H$_4$Me)$_2$(μ-O)$_2${Me$_3$SiNC(Ph)NCH$_2$CH$_2$Me}$_2$] (12). A solution of [Ti(η-C_5H_4Me)(N*t*Bu){Me_3SiNC(Ph)NCH_2CH_2Me}] (**5**; 0.29 g, 0.67 mmol) in benzene (30 mL) was exposed to ca. 1 atm of CO_2 via a dual-manifold Schlenk line. The solution was stirred and immediately changed color from red-brown to cherry red and after 15 min turned brown. Volatiles were removed under reduced pressure to give a brown oil, which was triturated with pentane (20 mL) to give a brown waxy solid that was shown by NMR to be a mixture of two isomers, **12a** and **12b**. Yield: 0.135 g (37%).

IR data (KBr plates, Nujol mull, cm^{-1}): 1514 (m), 1488 (s), 1436 (s), 1356 (m), 1246 (m), 1184 (w), 1154 (w), 1106 (m), 1096 (m), 1036 (m), 962 (m), 902 (s), 870 (m), 836 (s), 798 (m), 752 (m), 702 (s), 620 (w). EI-MS: *m/z* 673 [M − C_5H_4Me]$^+$ 25%, *m/z* 233 [Me_3SiNC(Ph)$NCH_2CH_2CH_2$Me]$^+$ 32%. Anal. Found (calcd for $C_{38}H_{56}N_6O_2Si_2Ti_2$): C, 60.6 (60.6); H, 7.4 (7.5); N, 7.3 (7.4).

^{1}H NMR data for **12a** (C_6D_6, 500.1 MHz, 293 K): 7.2−7.0 (10H, m, C_6H_5), 6.62 (2H, m, 2- or 5-C_5H_4Me), 6.53 (2H, m, 5- or 2-C_5H_4Me), 6.29 (2H, m, 3- or 4-C_5H_4Me), 6.23 (2H, m, 4- or 3-C_5H_4Me), 3.27 (2H, m, CN_2CH_2), 3.11 (2H, m, CN_2CH_2), 2.35 (6H, s, C_5H_4*Me*), 1.60 (4H, m, C*H*$_2$CH$_3$), 0.65 (4H, t, CH_2CH_3, ^3J = 13.2), 0.16 (18H, s, $SiMe_3$). ^{13}C{^{1}H} NMR data for **12a** (C_6D_6, 125.7 MHz, 293 K): 173.64 (CN_2), 136.62 (*i*-C_6H_5), 128.65, 128.45, 128.30, 126.94 (C_6H_5), 114.17 (2- or 5-C_5H_4Me), 113.01 (3- or 4-C_5H_4Me), 112.53 (4- or 3-C_5H_4Me), 112.06 (5- or 2-C_5H_4Me), 57.97 (CN_2CH_2), 47.11 (C_5H_4*Me*), 29.84 or 29.66 (*C*H_2CH$_3$), 15.79 (CH_2CH_3), 2.85 ($SiMe_3$). 1 × C_6H_5 and 1-*C*$_5$H$_4$Me not observed. ^{1}H NMR data for **12a** (CD_2Cl_2, 500.1 MHz, 293 K): 7.4−7.5 (10H, m, C_6H_5), 6.28 (4H, m, 3- and 4-C_5H_4Me), 6.03 (4H, s, br, 2- and 5-C_5H_4Me), 2.99 (2H, m, CN_2CH_2), 2.87 (2H, m, CN_2CH_2), 2.19 (6H, s, C_5H_4*Me*), 1.43 (4H, m, C*H*$_2$CH$_3$), 0.71 (6H, t, CH_2CH_3, ^3J = 7.3), −0.16 (18H, s, $SiMe_3$). ^{1}H NMR data for **12b** (C_6D_6, 500.1 MHz, 293 K): 7.0−7.2 (m, 6H, C_6H_5), 3.27 (m, 2H, CN_2CH_2), 3.11 (m, 2H, CN_2CH_2), 2.34 (s, 6H, C_5H_4*Me*), 1.60 (4H, m, C*H*$_2$CH$_3$), 0.78 (6H, t, CH_2CH_3, ^3J = 7.3), 0.15 (18H, s, $SiMe_3$). ^{13}C{^{1}H} NMR data for **12b** (C_6D_6, 125.7 MHz, 293 K): 173.58 (CN_2), 136.64 (*i*-C_6H_5), 128.62, 127.92, 127.34, 126.87, 126.82 (C_6H_5), 114.02 (2- or 5-C_5H_4Me), 113.26 (3- or 4-C_5H_4Me), 112.73 (4- or 3-C_5H_4Me), 112.44 (5- or 2-C_5H_4Me), 57.86 (CN_2CH_2), 45.53 (C_5H_4*Me*), 29.84 or 29.66 (*C*H_2CH$_3$), 15.79 (*CH$_2$CH3*), 2.80 ($SiMe_3$), 1-C_5H_4Me not observed. ^{1}H NMR data for **12b** (CD_2Cl_2, 500.1 MHz, 293 K): 7.4−7.5 (10H, m, C_6H_5), 6.21 (4H, m, 3- and 4-C_5H_4Me), 6.03 (4H, s, br, 2- and 5-C_5H_4Me), 2.99 (2H, m, CN_2CH_2), 2.87 (2H, m, CN_2CH_2), 2.19 (6H, s, C_5H_4*Me*), 1.43 (4H, m, C*H*$_2$CH$_3$), 0.71 (6H, t, CH_2CH_3, ^3J = 7.3), −0.13 (18H, s, $SiMe_3$).

NMR Tube Scale Synthesis of [Ti(η-C$_5$H$_4$Me){OC(O)N*t*Bu}{Me$_3$SiNC(Ph)NCH$_2$CH$_2$CH$_2$NMe$_2$}] (13). A solution of [Ti(η-C_5H_4Me)(N*t*Bu){Me_3SiNC(Ph)$NCH_2CH_2CH_2NMe_2$}] (**4**; 20 mg, 4.2 μmol) in CD_2Cl_2 (0.5 mL) at −78 °C in a 5 mm NMR tube was exposed to ca. 1 atm of CO_2 via a dual-manifold Schlenk line. The brown solution immediately became cherry red. The ^{1}H NMR spectrum recorded at −78 °C after 5 min showed quantitative formation of **13**.

^{1}H NMR data (CD_2Cl_2, 500.1 MHz, 195 K): 7.40 (2H, app s, br, *o*- or *m*-C_6H_5), 7.32 (1H, app s, br, *p*-C_6H_5), 7.16 (2H, app d, *o*- or *m*-C_6H_5, app *J* = 5.50), 6.84 (1H, s, 3- or 4-C_5H_4Me), 6.39 (2H, s, 2- or 5- and 4- or 3-C_5H_4Me), 6.09 (1H, s, 5- or 2-C_5H_4Me), 3.23 (1H, m, CN_2CH_2), 3.06 (1H, m, CN_2CH_2), 2.30 (3H, s, C_5H_4*Me*), 2.02 (1H, m, C*H*$_2$NMe$_2$), 1.89 (1H, m, C*H*$_2$NMe$_2$), 1.53 (6H, s, NMe_2), 1.41, (2H, m, $CH_2CH_2CH_2$), 1.15 (9H, s, CMe_3), −0.27 (9H, s, $SiMe_3$). ^{13}C{^{1}H} NMR data (CD_2Cl_2, 75.5 MHz, 195 K): 171.96 (NC(O)O), 158.33 (CN_2), 132.79 (*i*-C_6H_5 or 1-C_5H_4Me), 131.99 (1-C_5H_4Me or *i*-C_6H_5), 128.93 (*o*- or *m*-C_6H_5), 128.34 (*o*- or *m*-C_6H_5), 128.04 (*p*-C_6H_5), 126.25 (*o*- or *m*-C_6H_5), 125.64 (*o*- or *m*-C_6H_5), 118.07 (2- or 5-C_5H_4Me), 117.48 (5- or 2- or 3- or 4-C_5H_4Me), 116.70 (5- or 2- or 3- or 4-C_5H_4Me), 116.04 (4- or 3-C_5H_4Me), 56.89 (*C*H_2NMe$_2$), 56.45 (*C*Me$_3$), 47.27 (CN_2CH_2), 44.31 (NMe_2), 29.32 (C*Me*$_3$), 28.46 ($CH_2CH_2CH_2$), 15.39 (C_5H_4*Me*), 0.76 ($SiMe_3$).

NMR Tube Scale Synthesis of [Ti(η-C$_5$H$_4$Me){OC(O)N*t*Bu}{Me$_3$SiNC(Ph)NCH$_2$CH$_2$Me}] (14). A solution of [Ti(η-C_5H_4Me)(N*t*Bu){Me_3SiNC(Ph)NCH_2CH_2Me}] (**5**; 23 mg, 5.3 μmol) in CD_2Cl_2 (0.5 mL) at −78 °C in a 5 mm NMR tube was exposed to ca. 1 atm of CO_2 via a dual-manifold Schlenk line. The brown solution immediately became cherry red. The ^{1}H NMR spectrum recorded at −78 °C after 5 min showed quantitative formation of **14**.

^{1}H NMR data (CD_2Cl_2, 500.1 MHz, 195 K): (7.30−7.42, 3H, m, *o*- or *m*-C_6H_5 and *p*-C_6H_5), 7.05−7.08 (2H, m, *o*- or *m*-C_6H_5), 6.85 (1H, s, 3- or 4-C_5H_4Me), 6.44 (1H, s, 2- or 5- or 4- or 3-C_5H_4Me), 6.41 (1H, s, 2- or 5- or 4- or 3-C_5H_4Me), 6.11 (1H, s, 5- or 2-C_5H_4Me), 3.09 (1H, m, CN_2CH_2), 2.94 (1H, m, CN_2CH_2), 2.30 (3H, s, C_5H_4*Me*), 1.49 (1H, m, C*H*$_2$Me), 1.34 (1H, m, C*H*$_2$Me), 1.15 (9H, s, CMe_3), 0.60 (3H, t, CH_3, ^3J = 7.32), −0.29 (9H, s, $SiMe_3$). ^{13}C{^{1}H} NMR data (CD_2Cl_2, 75.5 MHz, 195 K): 172.15 (NC(O)O), 158.50 (CN_2), 133.12 (*i*-C_6H_5 or 1-C_5H_4Me), 132.30 (1-C_5H_4Me or *i*-C_6H_5), 128.93 (*o*-, *m*-, or *p*-C_6H_5), 128.32 (*o*-, *m*-, or *p*-C_6H_5), 128.10 (*o*-, *m*-, or *p*-C_6H_5), 126.24 (*o*- or *m*-C_6H_5), 125.77 (*o*- or *m*-C_6H_5), 118.33 (2- or 5-C_5H_4Me), 117.53 (5- or 2- or 3- or 4-C_5H_4Me), 116.69 (5- or 2- or 3- or 4-C_5H_4Me), 116.22 (4- or 3-C_5H_4Me), 56.96 (*C*Me$_3$), 51.47 (CN_2CH_2), 29.42 (C*Me*$_3$), 24.64 (CH_2CH_3), 15.38 (CH_2CH_3), 11.06 (C_5H_4*Me*), 0.73 ($SiMe_3$).

NMR Tube Scale Synthesis of [Ti(η-C$_5$H$_4$Me){OC(O)N*t*Bu}{Me$_3$SiNC(Ph)NCH$_2$CH$_2$NMe$_2$}] (15). A solution of [Ti(η-C_5H_4Me)(N*t*Bu){Me_3SiNC(Ph)$NCH_2CH_2NMe_2$}] (**3**; 24 mg, 5.2 μmol) in CD_2Cl_2 (0.5 mL) at −78 °C in an NMR tube equipped with a J. Young valve was exposed to ca. 1 atm of CO_2 via a dual-manifold Schlenk line. The sample was warmed to −35 °C until the ^{1}H NMR spectrum showed quantitative

formation of **15** (ca. 10 min) and then cooled back down to −78 °C, at which temperature NMR data were collected.

^{1}H NMR data (CD_2Cl_2, 500.1 MHz, 195 K): 7.43 (3H, app s, br, *o*- or *m*-C_6H_5 and *p*-C_6H_5), 7.16 (2H, app d, *o*- or *m*-C_6H_5, app $J = 21.48$), 6.89 (1H, s, 3- or 4-C_5H_4Me), 6.44 (2H, s, 2- or 5- and 4- or 3-C_5H_4Me), 6.14 (1H, s, 5- or 2-C_5H_4Me), 3.22 (1H, m, CN_2CH_2), 3.16 (1H, m, CN_2CH_2), 2.30 (3H, s, C_5H_4Me), 2.26 (1H, m, CH_2NMe_2), 2.19 (1H, m, CH_2NMe_2), 1.90 (6H, s, NMe_2), 1.14 (9H, s, CMe_3), −0.30 (9H, s, $SiMe_3$). ^{13}C{^{1}H} NMR data (CD_2Cl_2, 75.5 MHz, 195 K): 172.59 (NC(O)O), 158.37 (CN_2), 133.54 (*i*-C_6H_5 or 1-C_5H_4Me), 131.99 (1-C_5H_4Me or *i*-C_6H_5), 129.01 (C_6H_5), 128.29 (C_6H_5), 128.04 (C_6H_5), 126.18 (C_6H_5), 125.99 (C_6H_5), 118.74 (2- or 5-C_5H_4Me), 117.27 (3- or 4-C_5H_4Me), 116.86 (5- or 2- or 4- or 3-C_5H_4Me), 116.68 (5- or 2- or 4- or 3-C_5H_4Me), 59.20 (CMe_3), 56.92 (CH_2NMe_2), 47.42 (CN_2CH_2), 45.05 (NMe_2), 29.56 (CMe_3), 15.38 (C_5H_4Me), 0.77 ($SiMe_3$).

Kinetic Studies of the Cycloaddition Reaction of 3 with CO_2. A standard solution of [Ti(η-C_5H_4Me)(N^{t}Bu)-{$Me_3SiNC(Ph)NCH_2CH_2NMe_2$}] (**3**) was prepared (11.5 mg, 25.0 μmol) with 1.5 equiv of 1,4-dimethoxybenzene (5.4 mg, 37.0 μmol) in CD_2Cl_2 (4.8 mL). Aliquots (0.6 mL) of this solution were transferred to 5 mm NMR tubes equipped with J. Young Teflon valves. The solutions were freeze−pump−thawed three times and cooled to −78 °C. Samples were exposed to CO_2 at pressures of 0.25, 0.50, 0.75, and 1.0 atm (>10-fold excess CO_2 at the lowest pressure studied) via a calibrated gas manifold. Samples were transferred to an NMR spectrometer maintained at a probe temperature of −78 °C and then warmed to −35 °C. ^{1}H NMR spectra were recorded at 3 min intervals until >90% of **3** had been consumed (8 h for 0.25 atm of CO_2, 2 h for 1 atm of CO_2).

Kinetic Studies of the Extrusion of ^{t}BuNCO from Carbamate Compounds 13−15. Solutions of **3**−**5** at 1.98 mol dm^{-3} concentration (5.2 mg (**3**), 5.4 mg (**4**), 4.9 mg (**5**), 11.4 μmol) with ca. 1.5 equiv of 1,4-dimethoxybenzene (2.3 mg, 16 μmol) in CD_2Cl_2 (0.6 mL) were prepared and transferred to 5 mm NMR tubes equipped with J. Young Teflon valves. The solution was freeze−pump−thawed three times and cooled to −78 °C. Samples were exposed to CO_2 at ca. 1.0 atm pressure (>10-fold excess CO_2) via a dual-manifold Schlenk line. Samples were transferred to an NMR spectrometer maintained at −78 °C and warmed to −30 °C, at which point all of the imido starting materials **3**−**5** had been consumed and only the carbamate compounds **13**−**15** were present. ^{1}H NMR spectra were recorded at 3 min intervals until >90% of **13**−**15** had been consumed (ca. 4 h for **13** and **14**, ca. 2 h for **15**). Experiments were carried out in duplicate for **13** and **15** at the same concentration. The "dummy-arm" system **14** was examined at 1.9×10^{-8}, 2.9×10^{-8}, and 3.8×10^{-8} mol dm^{-3} concentrations (4.9 mg (11.4 μmol), 7.4 mg (17.4 μmol), and 9.8 mg (2.3 μmol), respectively, in 0.6 mL of CD_2Cl_2). N.B. In the case of the two-carbon linker system **15**, a small amount of imido starting material **3** was still present at −30 °C and the data obtained until this had been consumed were discarded.

Crystal Structure Determinations of [Ti(η-C_5Me_5)-{N^{t}BuC(O)O}-{$Me_3SiNC(Ph)NCH_2CH_2CH_2NMe_2$}] (7), *trans*-[$Ti_2$(η-$C_5H_4Me)_2$(μ-O)$_2${$Me_3SiNC(Ph)NCH_2CH_2NMe_2$}$_2$] (10a), and *trans*-[$Ti_2$(η-$C_5H_4Me)_2$(μ-O)$_2${$Me_3SiNC(Ph)NCH_2CH_2NMe_2$}$_2$] (11a). Crystal data collection and processing parameters are given in Table 9. Crystals were mounted on a glass fiber using perfluoropolyether oil and cooled rapidly to 150 K under a stream of cold N_2 using an Oxford Cryosystems CRYOSTREAM unit. Diffraction data were measured using an Enraf-Nonius KappaCCD check diffractometer. Intensity data were processed using the DENZO package.[69] The structures were solved with SIR92,[70] and subsequent full-matrix least-squares refinements were carried out using CRYSTALS.[71] Coordinates and anisotropic thermal parameters of all non-hydrogen atoms were refined. Hydrogen atoms were placed in calculated positions. Full listings of atomic coordinates, bond lengths and angles, and displacement parameters for **7**, **10a**, and **11a** have been deposited at the Cambridge Crystallographic Data Center. See the guidelines for authors in the first issue of this year.

Table 9. X-ray Data Collection and Processing Parameters for [Ti(η-C_5Me_5){N^{t}BuC(O)O}-{$Me_3SiNC(Ph)NCH_2CH_2CH_2NMe_2$}] (7), *trans*-[$Ti_2$(η-$C_5H_4Me)_2$(μ-O)$_2${$Me_3SiNC(Ph)NCH_2CH_2NMe_2$}$_2$] (10a), and *trans*-[$Ti_2$(η-$C_5H_4Me)_2$(μ-O)$_2${$Me_3SiNC(Ph)NCH_2CH_2CH_2NMe_2$}$_2$] (11a)

	7	10a	11a
empirical formula	$C_{30}H_{50}N_4O_2SiTi$	$C_{40}H_{62}N_6O_2Si_2Ti_2$	$C_{42}H_{66}N_6O_2Si_2Ti_2$
fw	574.74	810.95	838.99
temp/K	150	150	150
wavelength/Å	0.710 73	0.710 73	0.710 73
space group	$P2_1/n$	$P\bar{1}$	$P\bar{1}$
a/Å	9.0352(3)	12.7045(4)	9.3597(2)
b/Å	20.1007(8)	16.1774(4)	10.7886(2)
c/Å	18.2507(7)	22.8120(8)	12.1749(3)
α/deg	90	108.200(1)	72.8419(8)
β/deg	104.140(2)	94.168(1)	76.2046(8)
γ/deg	90	90.162(2)	72.8192(9)
V/Å^3	3214.2(2)	4440.5	1106.74(4)
Z	4	4	1
d(calcd)/Mg m^{-3}	1.19	1.21	1.26
abs coeff/mm^{-1}	0.33	0.45	0.45
R indices ($I > 3\sigma(I)$)[a]	R1 = 0.0597 wR2 = 0.0496	R1 = 0.0522 wR2 = 0.0575	R1 = 0.0367 wR2 = 0.0387

[a] $R1 = \sum||F_o| - |F_c||/\sum|F_o|$; $wR2 = \{\sum w(|F_o| - |F_c|)^2/\sum(w|F_o|^2)\}^{1/2}$.

Computational Details. All calculations were performed with the Gaussian 98 set of programs[72] within the framework of hybrid DFT (B3PW91)[53,54] on the model systems CpTi(NMe)-{MeC(NR)(NR′)} (Cp = η^5-C_5H_5; R = R′ = Me; R = SiH_3, R′ = $CH_2CH_2NMe_2$; R = SiH_3, R′ = $CH_2CH_2CH_2NMe_2$) and their reactions with CO_2. The titanium atom was represented by the relativistic effective core potential (RECP) from the Stuttgart group (12 valence electrons) and its associated (8s7p6d)/[6s5p3d] basis set,[73] augmented by an f polarization function (α = 0.869).[74] The silicium atom was represented by RECP from the Stuttgart group and the associated basis set,[75] augmented by a d polarization function.[76] For the reference system where R = R′ = Me, a 6-31G(d,p) basis set was used for all the remaining atoms of the complex (C, H, N).[77] For

(69) Otwinowski, Z.; Minor, W. *Processing of X-ray Diffraction Data Collected in Oscillation Mode*; Academic press: New York, 1997.
(70) Altomare, A.; Cascarano, G.; Carrithers, J. R.; Betteridge, P. W.; Cooper, R. I. *J. Appl. Crystallogr.* **1994**, *27*, 435.
(71) Watkin, D. J.; Prout, C. K.; Carruthers, J. R.; Betteridge, P. W.; Cooper, R. I. CRYSTALS: Chemical Crystallography Laboratory, Oxford, U.K., 2001.
(72) Frisch, M. J.; Trucks, G. W.; Schlegel, H. B.; Scuseria, G. E.; Robb, M. A.; Cheeseman, J. R.; Zakrzewski, V. G.; Montgomery, J. A., Jr.; Stratmann, R. E.; Burant, J. C.; Dapprich, S.; Millam, J. M.; Daniels, A. D.; Kudin, K. N.; Strain, M. C.; Farkas, O.; Tomasi, J.; Barone, V.; Cossi, M.; Cammi, R.; Mennucci, B.; Pomelli, C.; Adamo, C.; Clifford, S.; Ochterski, J.; Petersson, G. A.; Ayala, P. Y.; Cui, Q.; Morokuma, K.; Malick, D. K.; Rabuck, A. D.; Raghavachari, K.; Foresman, J. B.; Cioslowski, J.; Ortiz, J. V.; Stefanov, B. B.; Liu, G.; Liashenko, A.; Piskorz, P.; Komaromi, I.; Gomperts, R.; Martin, R. L.; Fox, D. J.; Keith, T.; Al-Laham, M. A.; Peng, C. Y.; Nanayakkara, A.; Gonzalez, C.; Challacombe, M.; Gill, P. M. W.; Johnson, B. G.; Chen, W.; Wong, M. W.; Andres, J. L.; Head-Gordon, M.; Replogle, E. S.; Pople, J. A. *Gaussian 98*; Gaussian, Inc.: Pittsburgh, PA, 1998.
(73) Andrae, D.; Häussermann, U.; Dolg, M.; Stoll, H.; Preuss, H. *Theor. Chim. Acta* **1990**, *77*, 123.
(74) Ehlers, A. W.; Bohme, M.; Dapprich, S.; Gobbi, A.; Höllwarth, A.; Jonas, V.; Köhler, K. F.; Stegmann, R.; Veldkamp, A.; Frenking, G. *Chem. Phys. Lett.* **1993**, *208*, 111.
(75) Bergner, A.; Dolg, M.; Kuchle, W.; Stoll, H.; Preuss, H. *Mol. Phys.* **1993**, *30*, 1431.
(76) Hollwarth, A.; Bohme, H.; Dapprich, S.; Ehlers, A. W.; Gobbi, A.; Jonas, V.; Kohler, K. F.; Stagmann, R.; Veldkamp, A.; Frenking, G. *Chem. Phys. Lett.* **1993**, *203*, 237.
(77) Hariharan, P. C.; Pople, J. A. *Theor. Chim. Acta* **1973**, *28*, 213.

the mixed system (R = SiH_3), only the nitrogen atoms (even that of the chelated arm) and the carbon atoms of the Cp ring were represented by a 6-31G(d,p) basis set; the remaining atoms (C and H) were represented by a 6-31G basis set to save computational resources. For all systems, CO_2 was represented by 6-31G(d,p) basis sets. The ONIOM calculations[78] were performed on the experimental systems **3**, **3′**, **4**, and **4′** and the Ph group as well as the Me groups on Si and on the imido ligand were treated at the MM level using the UFF force field.[79] The QM part was treated at the B3PW91 level, and the atoms were represented as described above. In both QM and ONIOM calculations, full optimizations of geometry without any constraint were performed, followed by analytical computation of the Hessian matrix to confirm the nature of the located extrema as minima or transition states on the potential energy surface. The nature of the transition states was checked by slightly perturbing the TS geometry along the TS vector in both directions and optimizing the resulting geometries as local minima to ensure the nature of the connected intermediates. Gibbs free energy values are given at $T = 298$ K unless otherwise stated, and the values at other temperatures were calculated using the *freqchk* utility in the Gaussian 98 package.

(78) Svensson, M.; Humbel, S.; Froese, R. D. J.; Matsubara, T.; Sieber, S.; Morokuma, K. *J. Phys. Chem.* **1996**, *100*, 19357.

(79) Rappé, A. K.; Casewitt, C. J.; Colwell, K. S.; Goddard, W. A.; Skiff, W. M. *J. Am. Chem. Soc.* **1992**, *114*, 10024.

Acknowledgment. We thank the EPSRC and the CNRS for support and Professor J. D. Protasiewicz for helpful discussions. E.C. and P.M. thank the Royal Society of Chemistry for International Authors Travelling Grants. We acknowledge the use of the EPSRC National Service for Computational Chemistry Software and the UK Computational Chemistry Facilty. We thank the British Council for an Alliance grant.

Supporting Information Available: X-ray crystallographic files in CIF format for the structure determinations of **9**, **10a**, and **11a**, graphs used for the determination of kinetic parameters, and tables giving further details of the DFT calculations. This material is available free of charge via the Internet at http://pubs.acs.org.

OM049026F